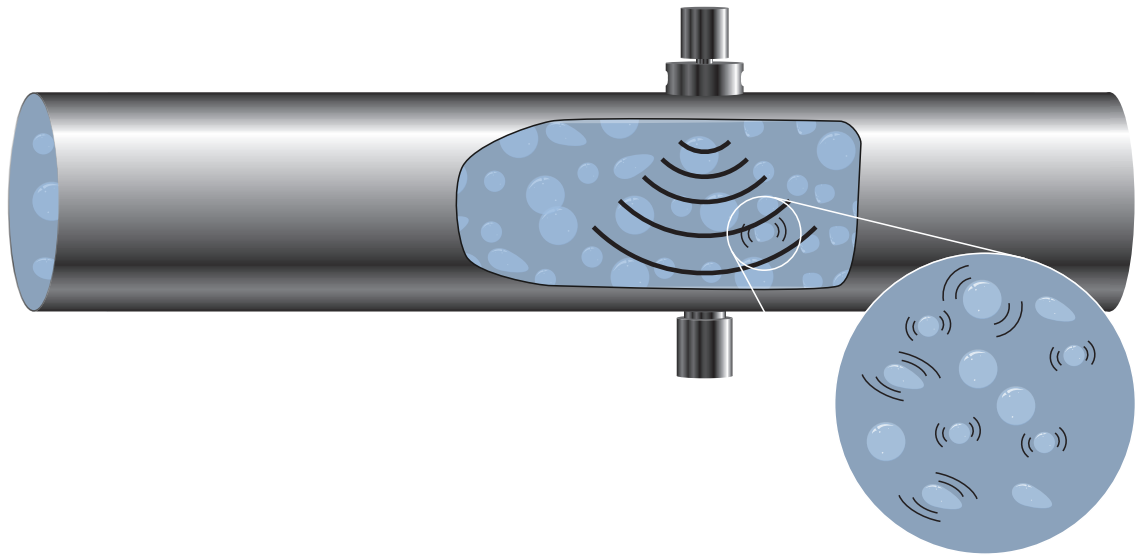


CHALMERS



Modelling Transferability in Active Acoustic Spectroscopy

Master of Science thesis in COMPLEX ADAPTIVE SYSTEMS *and*
ENGINEERING PHYSICS

Magnus GYLLENHAMMAR

Department of Signals and Systems

CHALMERS UNIVERSITY OF TECHNOLOGY
Gothenburg, Sweden 2016

Master's Thesis SSYX04-EX016/2016



Fraunhofer

CHALMERS
Research Centre
Industrial Mathematics

MASTER'S THESIS EX016/2016

Modelling Transferability in Active Acoustic Spectroscopy

Magnus GYLLENHAMMAR



CHALMERS
UNIVERSITY OF TECHNOLOGY



Fraunhofer **CHALMERS**
Research Centre
Industrial Mathematics

Department of Signals and Systems
CHALMERS UNIVERSITY OF TECHNOLOGY

Gothenburg, Sweden 2016

Modelling Transferability in Active Acoustic Spectroscopy

Magnus Gyllenhammar

© Magnus Gyllenhammar, 2016.

Examiner: Tomas McKelvey

Master's thesis EX016/2016
Department of Signals and Systems
CHALMERS UNIVERSITY OF TECHNOLOGY
SE-412 96 Göteborg
Sweden
Telephone + 46 (0)31-772 1000

TITLE PAGE:

A schematic illustration of the Acospector with the sound emitter and a force sensor on top of the pipe and with a collector on the diametrically opposite side of the pipe, measuring the sound that has traveled through the pipe with the process fluid.

Tryckeriets namn
Gothenburg, Sweden 2016

Modelling Transferability in Active Acoustic Spectroscopy

Project code: SSYX04-EX016/2016

Author:

Magnus GYLLENHAMMAR
maggy1@student.chalmers.se

Examiner:

Tomas MCKELVEY

Supervisor:

Fredrik EKSTEDT

Modelling Transferability in Active Acoustic Spectroscopy

Magnus Gyllenhammar
Department of Signals and Systems
CHALMERS UNIVERSITY OF TECHNOLOGY

Abstract

This thesis has investigated the Acospector, an active acoustic spectroscopy system produced by the Swedish company Acosense. The purpose was to find a transferability model of the system, such that the calibration time at (re)installation of the system could be reduced. Through theoretical investigations of the viscous wave equation for suitable geometries an experimental plan was devised in order to find a working transferability model.

It was concluded that component-wise first order linear multiplicative and additive models were insufficient for the task of finding the transferability of the system. Further frequency shift models through compositions could be rejected on the grounds of insufficient capabilities to capture the complexity of the system. Based on the theoretical investigation of the viscous wave equation, together with the conducted experiments, it could be concluded that the system is susceptible to changes in the mounting positions of the components as well as changes in certain media parameters.

Future work into the transferability of the system is proposed to focus on new ways of using the system, be that in terms of the signals used or the mounting set up. These might provide sufficiently simple transferability models for practical and valuable purposes.

Keywords: acoustics, active acoustic spectroscopy, modelling, transferability, viscous wave equation, spectroscopy, spectra, transfer-function, frequency analysis, digital waveguide, chemometrics

Modellering av transferbarhet i aktiv akustisk spektroskopi

Magnus Gyllenhammar
Avdelningen för Signaler och System
CHALMERS TEKNISKA HÖGSKOLA

Sammanfattning

Detta exjobb har undersökt instrumentet Acospector, ett instrument baserat på aktiv akustisk spektroskopi och som tillverkas av det svenska företaget Acosense. Syftet med projektet var att hitta en transferbarhetsmodell för systemet, sådan att (om)installationstiden för systemet kunde bli minskad. Genom teoretiska undersökningar av den viskösa vågekvationen, för några passande geometrier, utformades en experimentell plan med fokus på att avgöra transferbarheten och hitta en fungerande och implementerbar lösning.

Slutsaten är att första ordningens komponentvisa linjära multiplikativa och additiva modeller inte är tillräckliga för att modellera transferbarheten i systemet. Vidare kunde även sammansatta modeller förkastas baserat på deras otillräckliga förmåga att fånga komplexiteten i systemet. Baserat på den teoretiska undersökningen av den viskösa vågekvationen, tillsammans med de utförda experimenten kunde det troliggöras att liknande system påverkas av förändringar i monteringspositionen av komponenterna samt av mediets parametrar.

Vidare undersökningar av transferbarheten av systemet föreslås utgå från nya sätt att använda systemet, inklusive nya monteringsuppsättningar och ljudinsignaler. Dessa förändringar skulle potentiellt kunna medföra att en både praktisk och värdefull transferbarhetsmodell kan åstadkommas.

Denna rapport är skriven på engelska.

Nyckelord: akustik, aktiv akustisk spektroskopi, modellerande, transferbarhet, spektroskopi, spektrum, överföringsfunktion, frekvensanalys, digital waveguide model, vågekvation, kemometri, viskös vågekvation

Preface

This thesis has been written during the spring of 2016 in collaboration with Fraunhofer-Chalmers Center (FCC) and Acosense. Being stationed at FCC this is where the main part of the work has been carried out, but site visits, including measurements of the real system have also been done to Acosense's office.

Acknowledgements

Firstly, I would like to thank Mats Jirstrand and FCC for the opportunity to write this thesis. It has been a great challenge and it has allowed me to gain a lot of new knowledge and insights into the field of acoustics as well as frequency analysis and signal processing. Secondly, a large token of appreciation goes to my supervisor, Fredrik Ekstedt, who has been of much help in discussing and directing the work over the semester. Emil Gustavsson has also provided invaluable input and insights into the process, as has Mats Jirstrand, Catarina Dudas and Mikael Wallman. Further I would like to direct thanks to Carl Jansson and Johannes Kocher at Acosense, who has showed me how to operate their equipment as well as giving me an understanding of how to best conduct measurements on the system. Their knowledge and expertise has really helped me move past a lot of hurdles during the course of the project.

Thank you all for your help and support!

Magnus GYLLENHAMMAR
Gothenburg, May 19, 2016

Abbreviations

To facilitate for the reader of this thesis a list of abbreviations used throughout the report follows.

Abbreviation	Definition
AAS	Active Acoustic Spectroscopy
CSD	Cross Spectral Density
DFT	Discrete Fourier Transform
FRF	Frequency Response Function
LTI	Linear time invariant
LSE	Least squares estimation
PLS	Partial Least Square
PSD	Power Spectral Density

Contents

1	Introduction	1
1.1	Background	2
1.2	Purpose and objectives	3
1.2.1	Definition of transferability	3
1.2.2	Limitations	4
2	Theory	5
2.1	Propagation of sound	5
2.1.1	Simple plane wave	6
2.1.2	Acoustic wave propagation in viscous fluids	6
2.1.3	The viscous wave equation in 3D	7
2.2	Acoustic spectroscopy	7
2.2.1	The ECAH theory	7
2.2.2	Applications	8
2.2.3	Passive acoustic spectroscopy	9
2.2.4	Active acoustic spectroscopy	9
2.3	Frequency analysis	10
2.3.1	Discrete Fourier Transform (DFT)	10
2.3.2	Spectral and cross-spectral densities	11
2.3.3	Frequency response function (FRF)	11
2.3.4	Band-pass filter	13
2.4	Digital waveguides	13
2.4.1	The delay line	13
2.4.2	Systems with losses	14
2.4.3	Open-ended tube with losses	14
2.4.4	Digital waveguide of the viscous wave equation	15
2.5	The LTI-assumption	17
2.6	Transfer models	17
2.6.1	Linear model	17
2.6.2	Frequency shift model	19
2.7	Parameter estimation	19
3	Simulation results	21

3.1	Frequencies in 1D	21
3.1.1	Dependence on ν	21
3.2	Digital waveguide	23
3.3	Frequencies in 3D	27
4	Experimental setup	29
4.1	Materials and setup	29
4.1.1	Parts used	31
4.2	Experimental design	31
4.3	Experimental procedure	32
4.3.1	Measurement series	32
4.4	System identification investigation	34
5	Results	35
5.1	Relative and absolute positions in water	35
5.2	With and without silicone bands	40
5.3	Water vs. air	41
5.4	Peak analysis	42
5.5	Measurement stability	44
5.5.1	Remounting of system	45
5.6	Evaluation of transferability models	47
5.6.1	Multiplicative model	47
5.6.2	Additive model	48
5.6.3	Frequency shift model	48
5.7	System parameter estimation	48
5.8	Measurements on salt water	51
6	Discussion	53
6.1	Transferability models	53
6.2	Comparison to theory	54
6.3	Measurement reliability	55
6.3.1	Sources of error	55
6.4	Information contained in the spectra	56
6.5	Future work	57
6.5.1	Transferability	57
6.5.2	Investigate alternative uses for the instrument	57
6.5.3	Develop alternative models for feature extraction	58
6.5.4	Relating the features to changes in the medium	59
7	Conclusions	61
	Bibliography	63
A	Wave solution 3D	65
A.1	Cylindrical system	65
A.1.1	Boundary conditions	67
A.1.2	Attenuation and resonance	67

B System identification	69
B.1 Linear optimisation	69

1

Introduction

UPTIME OF PRODUCTION SYSTEMS is an important factor for a system's profitability. Being able to ensure quality and reliability of such systems without interrupting production is thus a challenge with considerable impact on both profitability and efficiency. This challenge has been tackled in numerous different ways, spanning from off-line sampling, where a sample of the production fluid is extracted for off-site laboratory analysis, to optical spectroscopy. Using mechanical (acoustical) waves, rather than electromagnetic ones, to measure material properties has shown considerable promise, the main benefit being that acoustic waves are able to propagate through all types of fluids, unlike optical and other electromagnetic waves. Further, acoustic measurements do not require direct contact with or view of the fluid in question, but measurements can be carried out without interfering with the production, and measurement devices can be kept isolated from the production flow.

Acosense is a Swedish company that has started to deliver on this promise through their *Acospector Acoustic Chemometer*, which uses active acoustic spectroscopy (AAS) and chemometrics in the form of a partial least square (PLS) regression model to determine, measure and monitor several important fluid properties simultaneously. The product is currently used by customers in the pulp and paper industry as well as the pharmaceutical industry [3]. Setting up the Acospector includes a calibration procedure, where the system has to learn the characteristics of the fluid in question. This is done through using reference samples acquired from off-line laboratory analysis of the process fluid. The calibration and learning are not only affected by the fluid in the pipe, but also from the pipe itself as well as the mounting of the device and the surrounding environment. Some of these effects are negligible, but the dependence of the pipe and mounting of the system are not. Rather than having to repeat the whole calibration procedure each time the Acospector is (re)installed, the hope is to be able to reuse the already learnt properties of the fluid and partly remove the response obtained from the pipe and mounting system. This would not only decrease the time before the system can go

on-line as well as the number of off-line laboratory samples required to set up the PLS model, but it would also facilitate comparisons between production processes at different plants or locations.

This thesis focus on investigating this possibility and propose and evaluate a couple of different models to achieve transferability of the system between different mounting positions and system realisations. Starting with a theoretical investigation into the acoustic system itself an experimental plan was devised and carried out in order to obtain data for evaluating the transferability models.

1.1 Background

In 2001 a patent, *Active Acoustic Spectroscopy*, was filed by Liljenberg et al. for the benefit of ABB [19]. This patent was later, in 2007, handed over to Encubator AB, which in turn tasked Chalmers School of Entrepreneurship (CSE) with the commercialisation of the innovation [2]. This created the base of Acosense, which was founded in 2009 at CSE [2].

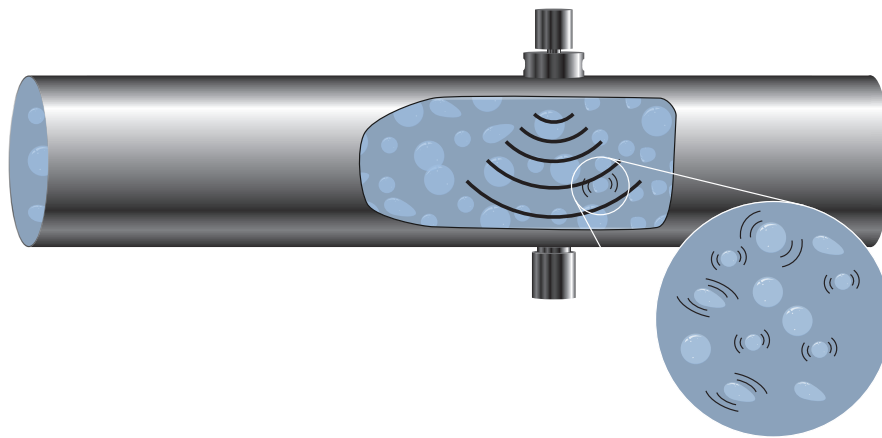


Figure 1.1: A schematic picture of the Acospector with the emitter at the top mounted on a force sensor to measure the input signal and a collector at the diametrically opposite side of the pipe. The emitter sends sound into the fluid that is excited and affects the sound that reach the opposite side of the pipe, where the collector measure the signal.

The device, Acospector, was developed based on the patent and it was first sold to EKA Chemicals in Bohus in 2010 [2]. A schematic picture of the device is shown in Figure 1.1. The device builds on the idea from the patent where an acoustic broadband signal is continuously emitted into the process fluid and the collected signal is compared to the initial signal to form the *Frequency Response Function* (FRF). The frequency response is used in conjunction with chemometrics in order to estimate the fluid parameters. The modelling of the system is in turn done by modelling reference values of the fluid through a partial least square (PLS) model on

the FRF. The modelling is done for each specific case and each specific installation. Some insights of fluid parameters and properties on a large scale can be used for new installations, but most of the modelling and tuning has to be redone when new devices are installed even if there is a robust and well functioning model that captures the properties in the fluid. The main reason for this is due to changes in the setup of each installation which affect the FRF of the system. Artifacts might be introduced due to new passive background noise in the production environment, whereas others might be due to changes in geometry of the pipe and the mounting of the system. The use of an appropriate estimate for the FRF (this is discussed further in the theory chapter) help to remove the environmental noise occurring in the system, so the main issues are the effects from geometry and mounting of the system, which can not be modelled as external noise.

1.2 Purpose and objectives

The purpose of this project is to investigate the possibility of separation of fluid and environmental components (including mounting and pipe) in the frequency spectrum from the AcoSpector, an active acoustic spectroscopy instrument, and by such determine the transferability of the system. Such a separation would help in reducing the calibration time for (re)installments of the system. The supervised learning method that precede the final instrument and which relate the acoustic spectra to the process fluid parameters is trained on data obtained through off line laboratory analysis of the process fluid. Providing a working solution for reducing the calibration time would in practise mean a method that transfers a working model from one system to an other without the need for a full (re)training of the model. Ideally a working solution of such a method should be provided with this thesis.

Further, a theoretical investigation is conducted in order to understand the underlying physics of the system. This understanding is used to focus the experimental investigations needed to obtain sufficient data for the transferability method evaluation. The working hypothesis is that a method based on relating measurements from different systems on a frequency-by-frequency basis should be sufficient to characterise the system.

1.2.1 Definition of transferability

Transferability is throughout this thesis used to signify the transfer of some model parameters from one system realisation to an other. It could be viewed as the mapping between one system realisation to the next which preserves the modelled aspects of the connections between fluid parameters and the transfer-function responses measured by the system.

1.2.2 Limitations

Due to the limited time available only the currently present measurement systems at Acosense are used, which in practise impose limitations to the variability of the system parameters. The lack of access to several, and especially continuously variable, media, pipe diameters as well as the lack of controllable parameters, such as temperature and pressure, pose clear limitations to what could reasonably be investigated. These limitations are also reflected in the width of the investigation as well as the generality of the results obtained. The focus of the thesis is to evaluate and ideally provide a transferability model for the current production system that is in operation by Acosense. Thus no effort is spent on alternative ways of using the system in order to acquire the transferability. Further, only transferability models of implementational and practical value are considered.

1.2.2.1 LTI assumption

The main assumption made throughout this thesis is that the active acoustic spectroscopy system can be considered *Linear time-invariant* (LTI).

2

Theory

FOLLOWING in this section is a presentation of some important theoretical concepts related to active acoustic spectroscopy (AAS) and which are of importance to this thesis. Starting off, is a discussion of the wave equation for acoustic waves and a case with an attenuation term appropriate for propagation in viscous fluids is presented. A sample solution is given and the resulting dispersion relationship is discussed. Next follows a section on the field of acoustic spectroscopy which start with presenting a theory for acoustic attenuation in heterogeneous systems. Some applications using acoustic spectroscopy to determine particle sizes over varying concentrations and with impurities are discussed and the field of passive acoustic spectroscopy is introduced. Concluding the second section is a discussion of AAS outlining the properties of this mode of acoustic spectroscopy as well as presenting further properties of the Acospector. Following that is a section on the background of frequency analysis and some tools related to this field, which is in turn followed by a section in which the digital waveguide model is investigate, primarily as a way of simulating the wave equation previously presented in a one dimensional geometry. Concluding the chapter are the sections on system modelling and parametrisation.

2.1 Propagation of sound

Sound is defined as "mechanical radiant energy that is transmitted by longitudinal pressure waves in a material medium and is the objective cause of hearing" [20]. Thus to understand how sound propagates through a medium one usually describe the motion of the longitudinal sound wave. In an idealistic, undamped case, the motion of a wave can be described by the following wave equation

$$\frac{\partial^2 u}{\partial t^2} = c^2 \nabla^2 u \quad (2.1)$$

in three dimensions, where u is the particle displacement and c is the sound velocity in the medium.

2.1.1 Simple plane wave

The general solution to equation (2.1) is on the form of a plane wave

$$u(\mathbf{r}, t) = A_0 e^{j(\mathbf{k}\mathbf{r} - \omega t + \varphi)}, \quad (2.2)$$

where A_0 is the amplitude, \mathbf{k} is the three dimensional wave vector, \mathbf{r} is the three dimensional spacial position, ω the angular frequency and φ is the phase shift. Using a combination of plane waves it is possible to solve very intricate problems with complex boundary conditions as well as initial conditions. By expanding the initial conditions and possible non-homogenities of the problem into their Fourier series, which are also on the form of plane waves, one can use these to form a viable solution to the posed problem [14, p. 109-111]. Restrictions on how the angular frequency relates to the wave vector might however come in and this is called the dispersion relation

$$\omega = \omega(\mathbf{k}). \quad (2.3)$$

This dispersion relation will place restrictions on how the wave can propagate through the medium. The simple wave equation presented in equation (2.1) will not give rise to such a restriction, but the situation presented in the following section, with a viscous attenuation term, will.

2.1.2 Acoustic wave propagation in viscous fluids

The equation for plane sound waves of small amplitude travelling in viscous media is given by [26]

$$\frac{\partial^2 u}{\partial t^2} = c^2 \frac{\partial^2 u}{\partial x^2} + \nu \frac{\partial}{\partial t} \frac{\partial^2 u}{\partial x^2}, \quad (2.4)$$

where ν is the kinematic viscosity coefficient inherent to the medium the sound is propagating through. The solution to the equation can be posed as a plane wave $u = u_0 e^{j(\omega t - kx)}$. Substituting that in the equation we get the following relation of ω and k

$$\omega^2 = k^2(c^2 + j\nu\omega), \quad (2.5)$$

and the dispersion relation becomes

$$k(\omega) = \pm \sqrt{\frac{\omega^2}{c^2 + j\nu\omega}} = \pm(\beta - j\alpha). \quad (2.6)$$

Solving this dispersion relation in terms of $\alpha(\omega)$ and $\beta(\omega)$ yields

$$\alpha(\omega) = \frac{\omega^2 \nu}{\sqrt{2\gamma(\omega)} (c^2 + \sqrt{\gamma(\omega)})} \quad \text{and} \quad \beta(\omega) = \sqrt{\frac{\omega^2}{2\gamma(\omega)} (c^2 + \sqrt{\gamma(\omega)})}, \quad (2.7)$$

where $\gamma(\omega) = c^4 + \omega^2\nu^2$. The full travelling wave solution to the equation can thus be written as

$$u(x, t) = A_0 e^{-\alpha(\omega)x} e^{j(\omega t - \beta(\omega)x)} \quad (2.8)$$

and we can see that the spatial propagation is dependent on the frequency of the sound, ω , as expected from the dispersion relation in equation (2.6). The attenuation constant $\alpha(\omega)$ forces the wave to decrease in amplitude as it propagates through the medium, whereas $\beta(\omega)$ change the phase of the wave as it propagates in x -direction.

Similarly to the case above this travelling wave solution can be used in order to comprise a composite solution to both zero and non-zero boundary and initial conditions. Assuming a pipe of length L with zero boundary conditions the term in βx expand to a sine or cosine and βL need to be a multiple of π (for equal boundary conditions, closed-closed or open-open) or $\pi/2$ (for different boundary conditions, closed-open). Using this we can find the fundamental frequencies of the system, by solving $\beta(\omega_n) = \frac{\pi n}{(2)L}$ for ω_n .

2.1.3 The viscous wave equation in 3D

For the more general case of three dimensions the wave equation of sound propagating in viscous fluids is given as

$$\frac{\partial^2 u}{\partial t^2} = c^2 \nabla^2 u + \nu \frac{\partial}{\partial t} \nabla^2 u, \quad (2.9)$$

which is solved for a three dimensional cylinder in Appendix A.1.

2.2 Acoustic spectroscopy

The frequency spectra resulting from sound having travelled through a medium can give interesting clues as to the properties of the medium. Specific frequencies being attenuated more than others hint of specific properties of the fluid such as size of particles suspended in the fluid, density as well as flow rate [13].

2.2.1 The ECAH theory

The ECAH theory, developed by Epstein and Carhart and further improved by Allegra and Hawley, lays the theoretical foundation for how different material parameters can be estimated from the attenuation of acoustic waves propagating through suspensions and emulsions [5, 11]. Attenuation of acoustical waves comes from six different sources or loss mechanisms, namely: (1) viscous, (2) thermal, (3) scattering, (4) intrinsic, (5) structural and (6) electrokinetic [8]. However, Allegra and Hawley find that in most cases, where long wave lengths in comparison to the particles'

sizes are considered, it is only the first four that make any significant contribution to the overall attenuation and that these additively make up the total attenuation α according to [5]

$$\alpha = \alpha_{vis} + \alpha_{th} + \alpha_{sca} + \alpha_{int}. \quad (2.10)$$

- (1) The **viscous** mechanism is related to the particle oscillations in the systems. These oscillations induce a shear wave between the particles and the medium and cause a loss of acoustic energy due to the shear friction between the oscillating particle and the medium [9]. For small rigid particles this is the dominant attenuation contributor [9].
- (2) **Thermal** losses are generated from temperature gradients present near the surface of the particles and are dominant in the attenuation for soft particles [9].
- (3) **Scattering** does not result in losses of acoustic energy, but the scattering will however redirect some of the sound and inhibit it from reaching the sound collector and will thus give rise to a perceived attenuation. Dukhin and Goetz find that this effect is significant only for high frequencies (> 10 MHz) and large particles ($> 3 \mu\text{m}$) [9].
- (4) The homogeneous phases of the particles and medium interact with the acoustic wave and give rise to the **intrinsic** mechanism of the attenuation. This effect needs to be considered when the over all attenuation is low [9].

In their model of acoustic attenuation Epstein and Carhart together with Allegra and Hawley start from the same fundamental laws, conservation of energy, momentum, mass and thermodynamic equations of state, as Stokes did when deriving (2.4). However, they considered suspensions and emulsions, which add an interactive coupling between the sound waves and the particles present in the medium as well as the medium itself. They assumed spherical particles of the same size, which further were present at relatively low concentration, compared to the fluid. In the long wave length regime they arrive at the final equations for how the different attenuation components relate to different properties of the medium. Further they validated their theoretical findings towards measurements on water particles suspended in air (fog) and found good correlation with the proposed theory [5, 11].

2.2.2 Applications

Despite the limiting assumptions of the ECAH model it has been used as a basis to predict particle sizes of systems with high concentrations (up to 50%) as well as for systems with impurities [4, 15]. The particle sizes that were possible to measure also spanned over a large range, from 10nm to 1mm [4], all challenging the assumptions made in the derivation of the theory. However, depending on the type of particles used these ranges differ considerably. If the particles tend to create clusters and stick together the model fails at much lower concentrations [15]. Using ultrasonic spectroscopy to determine particle size in suspensions is found to be a powerful

tool and many have explored different aspects of this with Babick et al. (2000) and Dukhin and Goetz (1996 and 2001) among others.

2.2.3 Passive acoustic spectroscopy

In addition to looking at the attenuation from emitted signals travelling through a medium it is also possible to listen to the sounds emitted from the process and medium itself during flow or production. This is what Esbensen et al. did for sand particles and PVC-granulates and they found that it was possible to monitor the particle processes by conducting multivariate analyses on the Fast Fourier Transform (FFT) of the collected noise signals from the process [12]. Further, Esbensen et al., investigated how this mode of passive listening to process noise can be used to determine flow rate and density for trace oil-in-water, jet-fuel and paper-pulp constituents, and also argued that flow regime is determinable by using this method [13].

2.2.4 Active acoustic spectroscopy

The *Acospector Acoustic Chemometer* that is the focus in this thesis is based on the principles outlined above, but actively emits sound into the process medium, and could thus be called an active acoustic spectroscopy (AAS) tool.

2.2.4.1 Acospector Acoustic Chemometer

An acoustic signal emitted into the medium is allowed to propagate through it and is collected by accelerometers close to the emitter, either on the opposite of the pipe. The emitter consists of a piezoelectric element that convert a digital signal into mechanical waves, which is the input signal to the system. To have an accurate measure of the signal amplitude at the emission the signal is passed through a force sensor before it is transmitted into the pipe. The output signal is compared to the input signal, as measured by the force sensor, and the *frequency response function* (FRF) is created. It is this FRF that constitute the main tool of analysis for the Acospector. In applications Acosense use a broad-band multi-sine signal ranging from 0 to 21 kHz with an approximate separation of 11.72 Hz. This choice of frequency regime mean that we are far from at the ultrasonic range, for which the ECAH-theory was developed and it is disputable how well the conclusions made by the ECAH-theory will apply to this regime. The scattering and intrinsic effects on attenuation could however, with high likelihood, be neglected in the analysis of the Acospector. Esbensen et al. in their investigation with passive acoustic spectroscopy, however, used a similar frequency regime and were also able to show that information exists in that regime.

2.3 Frequency analysis

Looking at a signal in itself might not at all be satisfactory in order to draw any relevant conclusions. The signal might appear noisy and without any apparent structure. One common way of analysing signals is to look at the frequencies that are contained within the signals. These frequencies will often give good indications of the components that make up the signal. Supporting frequency analysis is the theory of Fourier analysis. By the use of Fourier analysis any (sufficiently bounded and smooth) function can be expanded into a Fourier series, that completely describe the function in terms of Fourier coefficients [14, p. 213–225]. These coefficients are related to specific frequencies and it is by looking at these that the frequencies present in the function can be determined.

2.3.1 Discrete Fourier Transform (DFT)

Many times the signals that one wants to analyse are not known in terms of a specific analytic function, but the best one can do is sampling it in time. In order to further analyse the signal from these samples a common method is to use the *Discrete Fourier Transform* (DFT) of the signal. In much the same way as the ordinary Fourier Transform the DFT converts a time evolved signal into its frequency components. The DFT is the linear map on $\mathcal{F}_N : \mathbb{C}^N \rightarrow \mathbb{C}^N$ defined as [14, p. 251–253]

$$\mathcal{F}_N \mathbf{a} = \hat{\mathbf{a}}, \quad \hat{a}_m = \sum_{n=0}^{N-1} e^{-2\pi i m n / N} a_n \quad (0 \leq m < N), \quad (2.11)$$

where \mathbf{a} is the vector containing the samples of the signal and \mathbb{C}^N is the discrete space in which the sampled signal is bounded.

When sampling a function and applying the DFT one restricts the resolution in terms of frequency as well as the maximum frequency that can be caught in the transform. Suppose a sample frequency, $f_s = N/T$ is used, where T is the acquisition time of the samples and N is the number of samples taken. Then the maximum frequency that can be detected is the Nyquist frequency, $f_N = f_s/2$, according to the Nyquist sampling theorem. Further the resolution in frequencies of the transform is $df = 1/T = f_s/N$, which is only dependent on the acquisition time [21]. The acquired coefficients relate to the frequencies as $f_m = m f_s / N$ where m is the number of the component in the DFT. Due to the effect of aliasing higher frequencies could contribute to the obtained samples. Any sinusoid signal with frequency, f , will contribute to the amplitude measured at frequency, f_0 , if the number of cycles per sample differ with an integer, such that, given a sampling frequency, f_s , $f/f_s - f_0/f_s \in \mathbb{N}$. Thus it is important to minimise factors outside the frequency range of interest for any given sampling frequency.

2.3.2 Spectral and cross-spectral densities

One other way of acquiring the spectrum of a signal is by looking at the *power spectral density* (PSD). This is a spectral tool that accommodates random fluctuations in the signal. Despite being random, we require the signals to be stable, i.e. they have a constant expected value, at least over the period of observation. The PSD can be defined according to [25, pp. 6-7]

$$\phi_{xx}(\omega) = \sum_{k=-\infty}^{\infty} q_{xx}(k)e^{-j\omega k}, \quad (2.12)$$

where $q_{xx}(k)$ is the covariance of the time discrete signal, $x(t_i)$,

$$q_{xx}(k) = E \{x(t_i)x^*(t_i - t_k)\}. \quad (2.13)$$

The covariance is calculated as

$$q_{xx}(k) = \frac{1}{N-1} \sum_{i=1}^N x(t_i)x(t_i - t_k). \quad (2.14)$$

For two signals $x(t)$ and $y(t)$, both of which has an associated PSD, it is further possible to define the *cross-spectral density* (CSD) as

$$S_{xy}(\omega) = \sum_{\tau=-\infty}^{\infty} q_{xy}(\tau)e^{-j\omega\tau}, \quad (2.15)$$

where q_{xy} is the cross-correlation function of the two signals. The CSD can also be interpreted as the Fourier Transform of the cross-correlation function between the two signals.

2.3.3 Frequency response function (FRF)

In Figure 2.1 a schematic view of a linear system is shown in terms of the input signal, $X(\omega)$, the output, $Y(\omega)$, and the frequency response function, $H(\omega)$. The input signal $X(\omega)$ is sent into the system, which produces the output $H(\omega)X(\omega)$, which in turn is measured to $Y(\omega)$. The frequency response of the system can be obtained by normalising the output with the signal used for input according to

$$H(\omega) = \frac{Y(\omega)}{X(\omega)}, \quad (2.16)$$

where ω is the frequency of the emitted signal.

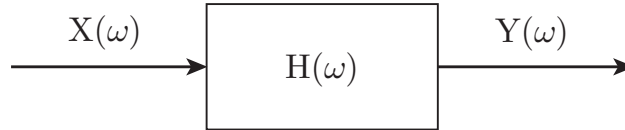


Figure 2.1: A linear system modelled with the transfer function $H(\omega)$. The input signal $X(\omega)$ produces the output signal $H(\omega)X(\omega)$, which is measured as the signal $Y(\omega)$.

In the idealised case the FRF will be the fraction between the output and the input as outline in equation (2.16). In reality this is seldom the case, there are often errors present both in the input as well as the output measurement. To mitigate the effect that these errors might have one might look at different estimates of the FRF. Following Rocklin et al. [23] we will now consider the H_1 and H_2 estimates of the FRF.

Suppose first that we have an error at the measurement of the output. This error might be coming from environmental noise, measurement errors or other sources. The output can thus be written as

$$Y(\omega) = H(\omega)X(\omega) + \epsilon, \quad (2.17)$$

where ϵ is the error. For notational simplicity it is assumed that X and Y are matrixes containing the input and responses of the system per frequency considered in the analysis. The H_1 estimator of the FRF is derived using the condition that the error ϵ should be uncorrelated with the input signal, such that the CSD between the error and the input, X , is zero. We can now multiply the transpose of the input signal matrix, X^T , to the right in equation (2.17). The expected value of this altered equation becomes

$$E \{ Y X^T \} = H E \{ X X^T \} + E \{ \epsilon X^T \} = H E \{ X X^T \}, \quad (2.18)$$

where the last equality holds true under the assumption that X is uncorrelated with ϵ , since this is in fact equivalent to $E \{ \epsilon X^T \} = 0$. Thus we acquire the H_1 estimate as

$$H_1 = S_{yx} S_{xx}^{-1}, \quad (2.19)$$

where again the S_{yx} is the CSD of the time domain signals $y(t)$ and $x(t)$ associated with the responses, X and Y . In the one-dimensional case the right-inverse will of course become a pure division between the two quantities on the right hand-side of the equations. Since we will have a single source in the case of the Acospector, we need only consider the one-dimensional case.

Similarly the H_2 estimate is derived using the assumption that the error is uncorrelated with the response, Y , and it becomes

$$H_2 = \frac{S_{yy}}{S_{xy}}, \quad (2.20)$$

in the one-dimensional case. There are several other estimates but we will restrict ourselves to these two.

At the present state Acosense primarily uses the H_1 estimate for their analyses.

2.3.4 Band-pass filter

In order to single out parts of a signal or a spectra one can use a band-pass filter. A band-pass filter lets frequencies within the given band pass through the filter, whereas the frequencies that fall outside the band are damped according to their distance to the critical frequencies of the band-pass filter. This could be of use when only certain aspects of the signal are of interest or when trying to extract specific frequency areas of the signal. Following Jaeger and Blalock a simple band-pass filter is constructed by combining a low-pass and a high-pass filter according to

$$BP(\omega) = LP(\omega)HP(\omega) = \frac{A_0}{(1 + \tau_c^{(low)} j\omega)} \frac{A_0 \tau_c^{(high)} j\omega}{(1 + \tau_c^{(high)} j\omega)}, \quad (2.21)$$

where A_0 is the amplification of the filters and τ_c is the inverse of the critical frequency of each filter $\omega_c = \tau_c^{-1}$ [16]. The critical frequency denote the frequency at which the filter has damped the signal with three decibels compared to the maximum amplitude.

2.4 Digital waveguides

The sound propagation in a system can be inferred from solving the partial differential equations of the system, including initial conditions and boundary conditions as well as possibly driving functions. It is generally possible to acquire a numerical solution to these equations, where the equation is solved on, for example, a grid of points. In most cases this might however be both difficult, as well as expensive in terms of computing power, especially since the grid spacing has to be less than half of the shortest wave length included in the investigation. Smith [24] presents an alternative way of computing the solutions to such problems. Rather than explicitly solving the equation for the physical variables in the system, he proposes the use of travelling waves and delay-lines to reproduce the behaviour of the system. He calls this model *Digital waveguides*.

2.4.1 The delay line

Since the investigation of le Rond d'Alembert (1747) [17] it has been known that the shape of a vibrating string can be fully described by two super-positioned waves travelling in opposite directions and it is on this insight that the delay line approached is based. This argument can also be extended to include other systems, such as tubes [24].

A visualisation of a loss-less delay line is presented in Figure 2.2.

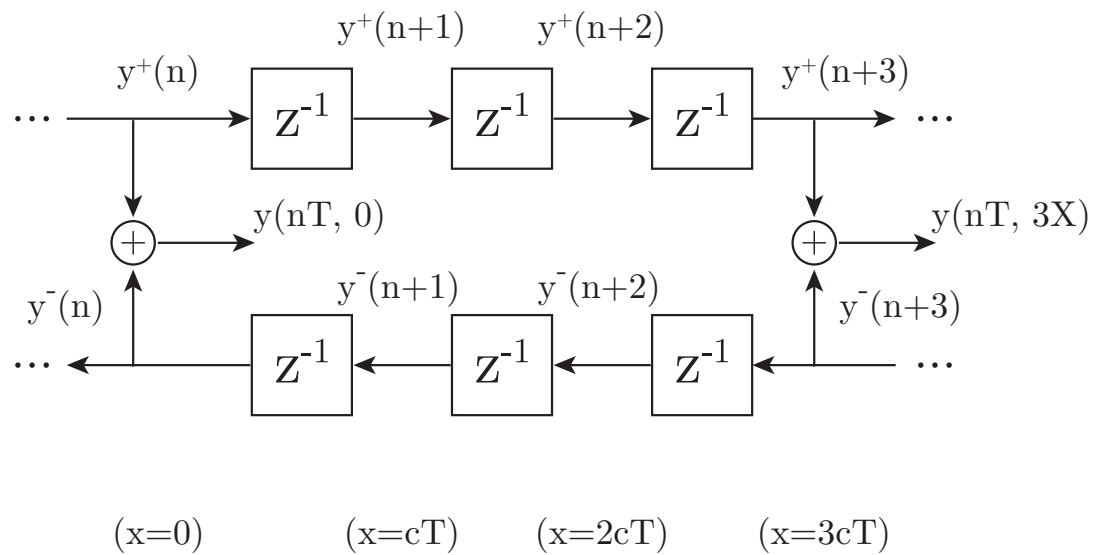


Figure 2.2: The set up of a digital simulation of a loss-less delay line. The z^{-1} denotes a *one-sample delay* and the y^+ and y^- are the waves travelling in positive and negative direction along the line. The setup has two observation points in $x = 0$ and $x = 3X = 3cT$ at which point the waves from the two directions are added to obtain the final signal. Here, familiarly, c is the sound velocity. (The figure is based on Figure 3 in [24]).

2.4.2 Systems with losses

However, the system of interest might very well not be loss-less and might even exhibit dispersion, with different propagation velocity for different frequencies. Thus, we must consider these effects and this is done by applying a filter to the signal. For a signal propagating a length l along the string (or tube) we can consider a filter that adds the effects of dispersion, phase shift and attenuation. Let $D(\omega)$ and $F(\omega)$ be such filters, where $D(\omega)$ is the delay due to time and $F(\omega)$ is the delay and attenuation due to the propagation distance $x = l$ through the medium.

If we further assume that the system is LTI we can lump all such filter together into one, for each section without a point of observation [7]. In the simple system depicted in Figure 2.2 the three z^{-1} could in such a manner be lumped together into one z^{-3} signifying a three-sample delay.

2.4.3 Open-ended tube with losses

To concretise the situation we can now consider a tube with open ends, in which we have a medium that affects the sound both dispersively as well as attenuatively. A figure of such a system is presented in Figure 2.3. At the ends we can assume that parts of the signal transmits out from the tube ($T(\omega)$), whereas the rest is reflected back into to system ($R(\omega)$). In the case of a rigid termination of a string (or a closed tube), this reflection is set to -1 and the transmission is thus zero. For the tube we can refer to Levine and Schwingers [18] investigations and conclude that the

reflection function, at least for an open pipe with air, can be approximated as

$$R(\omega) \approx \frac{-1}{1 + 2jka/\xi}, \quad (2.22)$$

where k is the wave number, a is the radius of the pipe and $\xi \approx 1$ is a scalar that determines the behaviour of the system as it transitions between the low to the high frequency region. Note that $a = 0$ reduces the system to closed ends with full reflection of $R = -1$.

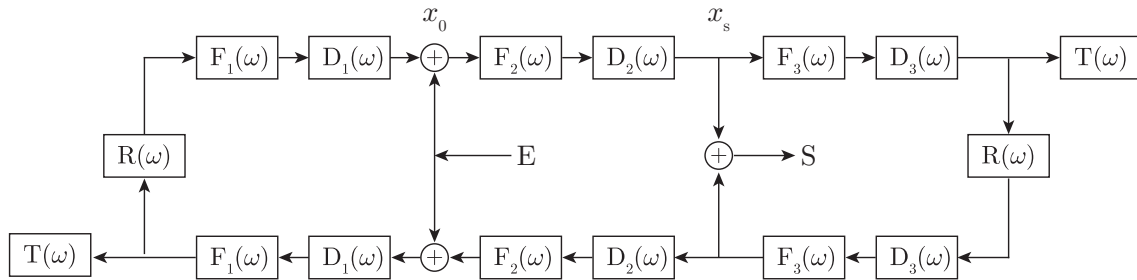


Figure 2.3: The delay line model of a tube with open ends being driven by the signal E at x_0 and where a signal S is measured at position x_s . The filters and delays for each of the sections are denoted F_i and D_i respectively. The sound transmission at the open ends is determined by the transfer function $T(\omega)$ and the reflection back into the pipe or tube by $R(\omega)$.

2.4.4 Digital waveguide of the viscous wave equation

In order to understand the transfer function that arise from emitting sound into a circular pipe with a viscous fluid flowing through it we will use the digital waveguide model outlined in the previous sections. First, however, we need to relate the filters and delays to the parameters of the wave equation (2.4). The delay filter is commonly selected as a pure time delay, such that $D_i(\omega) = e^{-j\omega d_i}$, where d_i is the propagation time through that particular section [7]. Since our travelling wave solution for the equation (2.4) seem to be separable it is fair to keep this separation and assignment of the filters even in our case. The filters, F_i can also be determined from the travelling wave solution given in equation (2.8), where $F(\omega)$ simply can be set to $F_i(\omega) = e^{j\omega d_i - j(\beta - j\alpha)l_i}$ with α and β given as in equation (2.7). l_i is the length of the section that the filter represent.

Since our system is a LTI system we can further use the trick of lumping filters together. Further we are only interested in the internal sound propagation and can thus neglect the transmission, $T(\omega)$, and focus only on the reflection, $R(\omega)$. Lumping all filters and delays together for each section of the delay line we obtain the system depicted in Figure 2.4.

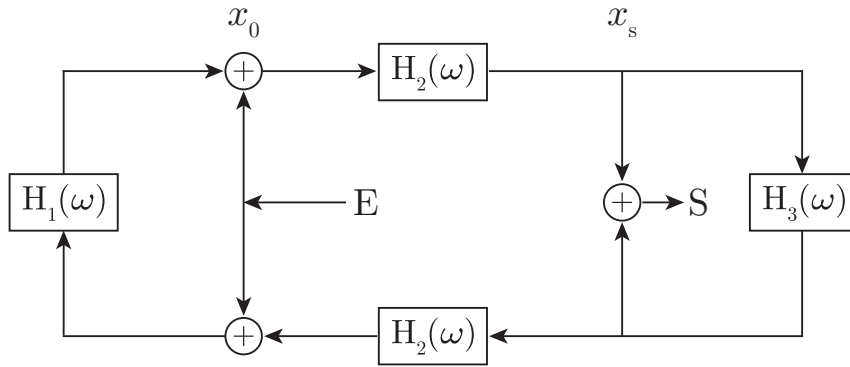


Figure 2.4: The final overview of the system after all filters and delays have been lumped together. The functions H_i are given in equation (2.23). The input signal is emitted at x_0 and the output is collected at x_s .

After lumping all filters shown in Figure 2.3 together we get the H_i :s in Figure 2.4 according to

$$\begin{cases} H_1 = D_1^2 F_1^2 R \\ H_2 = D_2 F_2 \\ H_3 = D_3^2 F_3^2 R \end{cases}, \quad (2.23)$$

where the dependence on ω has been omitted for notational simplicity. Further we can determine the lengths and propagation times for each of the filters according to

$$\begin{cases} l_1 = 2x_0 \\ l_2 = x_s - x_0 \\ l_3 = 2(L - x_s) \end{cases}, \quad (2.24)$$

given that the total length of the tube is L and that $x_0 < x_s$ and that $x_s < L$. The propagation times are given as $d_i = l_i/c$.

If we now assume that the signal is indeed emitted at x_0 and travel around the delay line and that the measurement of the output is conducted at x_s , we can construct the output transfer function as a sum of all possible sub paths from x_0 to x_s . There are four of these, two starting from the top left point of emission and two starting from the bottom left, each going to the two points of measurement of the output. Assuming that we seek a steady state solution, where the emitted signal is emitted continuously and where it has done so for a while, there will also be higher order terms added to this, where the wave has travelled an additional circuit along the delay-line. Let us denote the filter for one lap as $L_t = H_1 H_2^2 H_3$ and each of the sub paths G_i according to

$$\begin{cases} G_1 = H_2 & G_3 = H_1 H_2 \\ G_2 = H_2 H_3 & G_4 = H_1 H_2 H_3 \end{cases}. \quad (2.25)$$

Then the transfer function from input to output becomes

$$H(\omega) = \left(\sum_{i=0}^{\infty} L_t^i \right) \sum_{j=1}^4 G_j = \frac{\sum_{j=1}^4 G_j}{1 - L_t}, \quad (2.26)$$

where we in the last step have used the formula for geometric series. This is possible since, with a non-zero attenuation, we have $|L_t| < 1$. This solution is also what is acquired by analysing the circuit through using Kirchhoff's laws for electrical circuits for the four nodes of interest in Figure 2.4.

2.5 The LTI-assumption

By the *linearity* (L) we assume that the system can be described by a linear mapping, which transforms the input signal to the output signal of the system. And by *time-invariant* (TI) we mean that the system will produce the same response irrespective of when it is measured, given that the medium, geometry and environmental factors are held constant.

In the case of the Acospector it is to be expected that there will be a lot of fluctuations of the parameters in the system, also over a short time period. The fluctuations originate from the flow of the medium through the pipe and the fact that the processes measured are not completely perfect and stationary. However, even if these fluctuations give rise to differences in consecutive measurements they are due to physical changes in the system and medium. If these parameters would be held constant the TI assumption tells us that the response of the system should be consistent even if a measurement is carried out at an other day or hour. So, whenever the same combination of flow rates, medium and system setup reoccur the system should give the same response to the same input. That is the LTI assumption that underpins the workings of the system and the frequency analysis methods used throughout the thesis.

2.6 Transfer models

The way the sound propagates and interacts with the medium and pipe can be modelled in many different ways. Our objective is to find a simple enough model that allows for as few reference measurements as possible, but that still captures the essence of the system. If we assume that the system is built up by two parts, the geometry, pipe and environment and the medium we can postulate that each of these factors also contribute to the overall transfer function of the system. Assuming this is true and that the interaction of the sound with the two parts can be characterised as LTI systems there are a few easy models that should be able to capture these effects.

2.6.1 Linear model

Since the sound passes through the pipe, enters the medium and has to exit through the pipe in the opposite end the first model that comes to mind is a linear one, where each part of the system affect the sound. In addition to the sound propagating

through the medium it is conceivable that there is one component through which the sound only goes through the rim of the pipe. Together this amounts to

$$H_l^k = S_k V_l + T_k, \quad (2.27)$$

where H is the transfer function of the system, S_k and T_k are associated with the pipe, environment and the mounting of the system and where V_l models the effects of the medium. To be able to extract the information in the medium and separating that from the effects of the system, we need measurements on three different systems for three different media. Considering the purpose of providing a working system for practical implementation that reduce the number of laboratory samples needed this model can thus be rejected on the basis of not fulfilling the simplicity condition.

2.6.1.1 Multiplicative model

Reducing the linear model presented above we can consider $H_l^k = S_k V_l$, where H again is the transfer function of the system, S_k is the transfer function of the vessel part of the system, in system k , and V_l is the effects of the medium, for medium l . Let us assume an initial system $k = 0$ and a reference medium $l = 0$. First a measurement is carried out for this combination to acquire $H_0^0 = S_0 V_0$. Next the real medium, l , is fed into the system and measurements, $H_l^0 = S_0 V_l$, are obtained. To get rid of the system's impact we can construct the fraction between these two measurements

$$\frac{H_l^0}{H_0^0} = \frac{V_l}{V_0}, \quad (2.28)$$

which is independent on the system in which the measurements are collected. Using this quantity for the training of the system would pose a situation where the information about the medium could easily be passed from one system realisation to the next, by a simple measurement on the reference medium. This also implies that this fraction for any two systems should be equal if the same reference and measurement media are used, such that

$$\frac{H_l^k}{H_0^k} = \frac{V_l}{V_0} = \frac{H_l^m}{H_0^m} \quad (2.29)$$

for any systems k and m .

For this model it could further be reasonable to assume that additional linear effects come in and that the two fractions from two different systems are in fact related through a linear transform such that

$$\left(\frac{V_l}{V_0}\right)^{(1)} = c \left(\frac{V_l}{V_0}\right)^{(2)} + a, \quad (2.30)$$

for any constants $c, a \in \mathbb{R}$.

2.6.1.2 Additive model

A related model is an additive one, $H_l^k = S_k + V_l$, for which the division and multiplications are exchanged to subtraction and addition. The quantity of interest becomes $V_l - V_0$.

2.6.2 Frequency shift model

Based on the idea that changes in media parameters induce shifts of the resonance frequencies one further model to capture the transferability of the system is on the form of a composition $H_k^l = S_k \circ V_l$, where the medium function effectively skews and shifts the spectrum. It is important to recognise that the function for the medium has to be monotonically increasing, unless the peaks should be allowed to change order. In contrast to the previous models the composition does not have any simple quantity for comparison. Through measurements on the medium of interest and a reference medium it should be possible to construct the V_l that relate the reference measurements to the ones obtained on the medium of interest, such that

$$S_k \circ V_l = H_0^k. \quad (2.31)$$

Ideally the function, V_l , needed to relate the reference spectra to the one from the real medium should be equal for measurements on the same media in different systems.

2.7 Parameter estimation

A common practise when analysing systems and especially LTI systems is to try to find an applicable mathematical model to describe the observed effects [1]. A LTI system can, as mentioned before, be written on the form of the transfer function of the system

$$H(\omega) = \frac{Y(\omega)}{X(\omega)}, \quad (2.32)$$

where X and Y are the input and output respectively. This transfer function can usually, to satisfactory accuracy, be described by a fraction of two polynomials of suitable degrees.

Suppose we want to find a mathematical system representation in the frequency domain. Aarts outlines a procedure to achieve this, starting from the known (or measured) frequency response of the system at a number of angular frequencies, $\check{H}(\omega_k)$. One way of acquiring this response is to send a multi-sine signal through the system and transform and compare the response to the pure sine signals that were sent in. If it is a single-input-single-output LTI system that is under consideration this can be parametrised with two polynomials, just as discussed above

$$H(j\omega, \theta) = \frac{B(j\omega, \theta)}{A(j\omega, \theta)},$$

where θ is a parameter vector of the coefficients for the two polynomials. The posed problem of identifying a mathematical model of the system implies that we want to find the parameter vector, θ^* such that

$$\theta^* = \operatorname{argmin}_{\theta} \sum_{k=1}^N |\check{H}(\omega_k) - h(j\omega_k, \theta)|^2 |W(\omega_k)|^2,$$

where N is the number of frequencies in which we have measured the transfer function and where $W(\omega_k)$ is a suitable weighting function. Using our parametrisation from above and breaking out the polynomial in the denominator, A , we have the minimisation problem

$$\theta^* = \operatorname{argmin}_{\theta} \sum_{k=1}^N |A(j\omega_k, \theta)\check{H}(\omega_k) - B(j\omega_k, \theta)|^2 \frac{|W(\omega_k)|^2}{|A(j\omega_k, \theta)|^2}. \quad (2.33)$$

Using a fixed estimation for $A^*(\omega_k)$ allows us to turn this non-linear problem in the parameter θ into a linear problem on the form

$$\theta^* = \operatorname{argmin}_{\theta} \sum_{k=1}^N |A(j\omega_k, \theta)\check{H}(\omega_k) - B(j\omega_k, \theta)|^2 \frac{|W(\omega_k)|^2}{|A^*(j\omega_k)|^2}. \quad (2.34)$$

The non-linear problem can then be solved iteratively by considering the linear problem in equation (2.34). The solution to the problem is then used to update the estimate $A^*(\omega_k) = A(j\omega_k, \theta^*)$, which can then be used in the next iteration of the problem. This procedure is repeated until a reasonable level of convergence is reached. A least square estimate (LSE) to the linear problem in equation (2.34) is given in detail in Appendix B.1.

3

Simulation results

TO FORM A BASIC UNDERSTANDING of the system of interest a theoretical investigation has been conducted and this chapter will outline the findings from this investigation. Starting from the fundamental frequencies of the one-dimensional viscous wave equation, including the dependence on the viscosity ν , we continue to discuss the digital waveguide model and the results from those simulations. Concluding the chapter is a section relating to the wave solution in a cylinder and the fundamental frequencies of the different modes are discussed.

3.1 Frequencies in 1D

The fundamental frequencies to the model described in Section 2.1.2 can, as mentioned, be determined by equating the imaginary part of the exponent in x -direction to $n\pi/L$. If we assume that the pipe considered is terminated similarly in the two ends we also do not need the extra factor of two mentioned in Section 2.1.2. The equation to solve is

$$\beta(\omega_n) = \sqrt{\frac{\omega_n^2}{2\gamma(\omega_n)} \left(c^2 + \sqrt{\gamma(\omega_n)} \right)} = \frac{n\pi}{L}, \quad (3.1)$$

with $\gamma(\omega) = c^4 + \omega^2\nu^2$. Explicit solutions can be obtained through *Mathematica*, but they are too long to reproduce here, but we can make some analysis of results as well as produce a list of reasonable resonance frequencies that we would expect from the system.

3.1.1 Dependence on ν

In order to understand how the viscosity affect the resonance frequencies we can solve the above equation for several different values of ν and we thus get the results

presented in Figures 3.1 and 3.2. The first of the two figures present the increase of the fundamental frequency of the system with increasing viscosity for three different values of the system length, L , but with a fixed propagation speed of the sound, $c = 1484$ m/s.

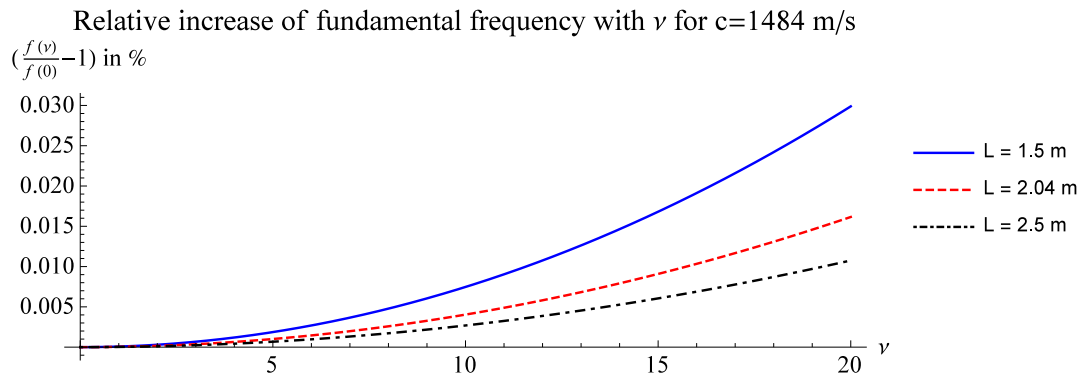


Figure 3.1: The change of the first resonance frequency relative to the fundamental frequency, $f(\nu = 0) = c/2L$, as the viscosity is changed for three different values of the system length, L , with the sound speed set to $c = 1484$ m/s. The changes are negligibly small for viscosities in the reasonable range, with relative differences to the fundamental frequency of less than one half of a per mille.

Figure 3.2 however, show the same increase in frequency with viscosity but for different sound speeds and for a fixed length, $L = 2.04$ m.

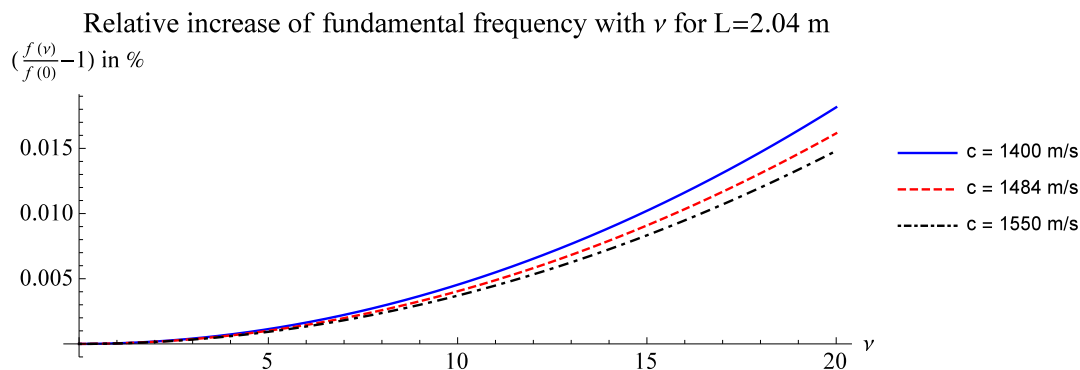


Figure 3.2: Shown is the first resonance frequency relative to the fundamental frequency, $f(\nu = 0) = c/2L$, change as the viscosity is changed for three different values of the sound speed, c , for fixed system length, $L = 2.04$ m. The changes are negligibly small for viscosities in the reasonable range, with relative differences to the fundamental frequency of less than one per mille.

As we see from the figures, for reasonable values of c , L and ν the change to the first fundamental frequency is less than one per mille and could, for all practical purposes, be omitted. This being said, the following resonance frequencies for $n > 1$ exhibit larger and larger change with increased viscosity. The extent of this relative change can be seen for five different frequencies, $n = \{1, 2, 5, 10, 15\}$, in Figure 3.3. The change is still small, but for $n > 10$ the relative difference approach $10^{-2} \approx 1\%$ already for small ν .

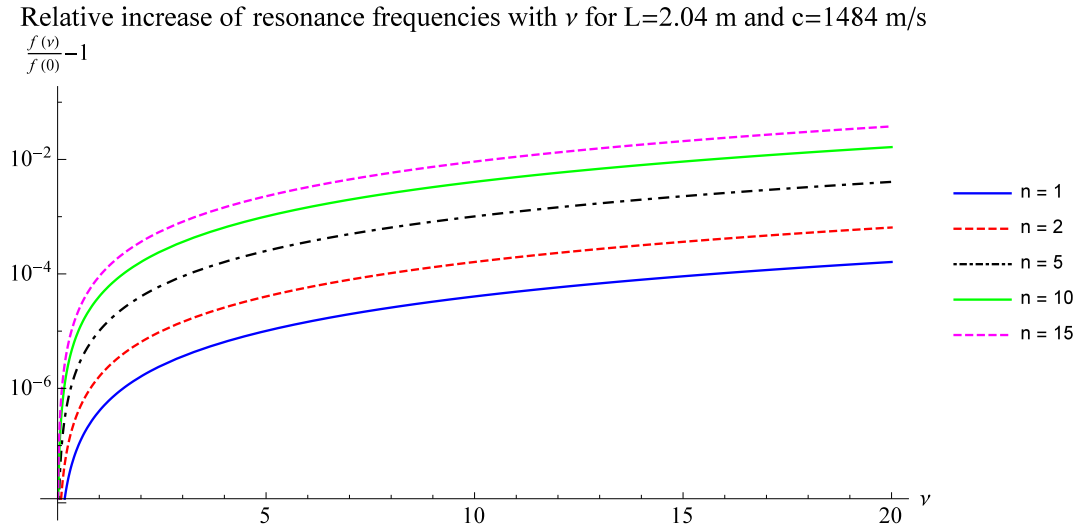


Figure 3.3: The relative change in resonance frequency between the fundamental frequencies, $f_n(\nu = 0) = cn/2L$, and the frequencies obtained from the viscous wave model. The sound speed is set to 1484 m/s and the length is 2.04 m. Here we can see that the rate of change with viscosity increase with higher numbers of n .

We can thus conclude that the resonance frequencies does indeed depend on the viscosity, but only to a limited extent and that the main factors contributing are the propagation speed of the sound together with the system length. These factors contribute as for the pure, non-viscous, case where the frequencies can be described by $f_m = \pi mc/L$.

3.2 Digital waveguide

Moving on to the digital waveguide model we can see similar tendencies in the results. The frequency peaks that appear are altered with changes in the system length and the propagation speed, but seem to remain constant for reasonable values of the viscosity. In the following analyses we consider a pipe with closed ends, since that is what is available for measurements at Acosense and it will thus be easier to compare the theoretical results from the ones obtained from the experiments. A closed end is easily modelled in the current waveguide model by setting the radius in the reflection filter, $a = 0$. The results that follow are acquired from implementing and running the model in MATLAB.

Figure 3.4 presents the magnitude of the transfer-functions from the digital waveguide simulations for two different values of the system length, L . Qualitatively the two transfer-functions looks the same, but with a shift corresponding to the new length of the system. Some of the peaks are however more damped for the smaller value of L , since the peak will be positioned at a higher frequency compared to the larger system and with the frequency dependent dampening, this peak will be more affected.

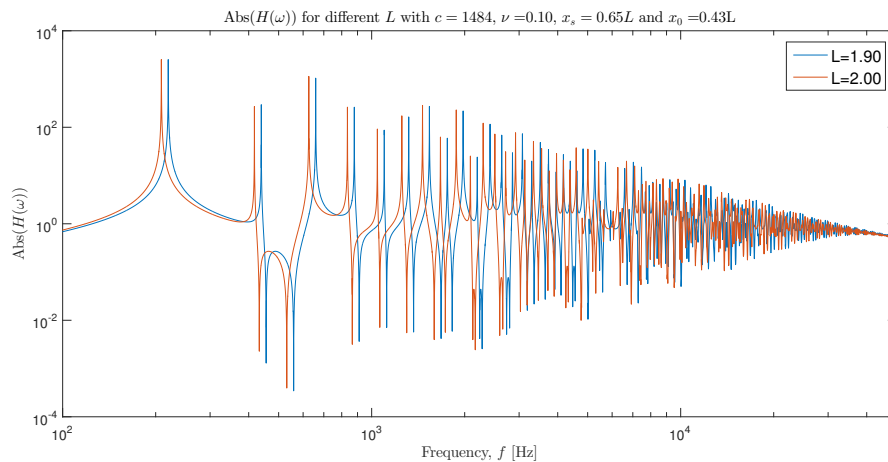


Figure 3.4: The results of the digital waveguide simulations for two different values of the system length, $L = \{1.9, 2\}$ m are presented. As we can see the whole transfer-functions are shifted with the change of the length.

Similarly for changes in propagation speed, c , the shift of the transfer-functions can be seen in Figure 3.5.

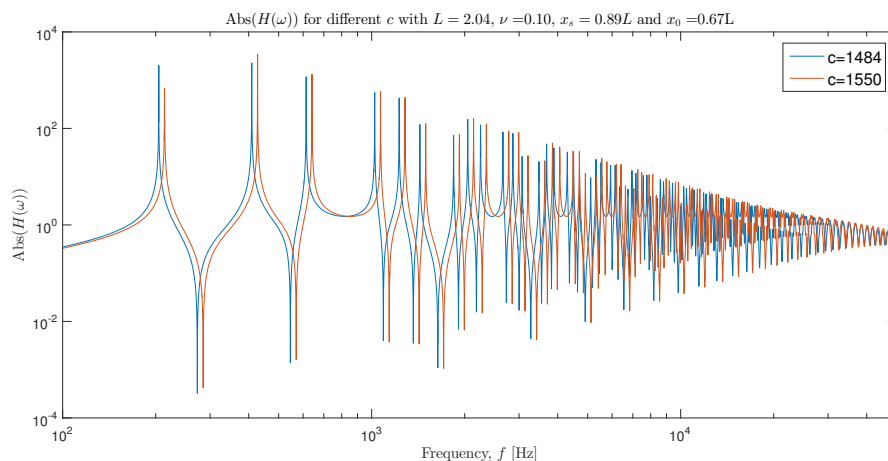


Figure 3.5: The results of the digital waveguide simulations with two different values of propagation speed, $c = \{1484, 1550\}$ m/s. As we can see the whole transfer-functions are again shifted with the change of c .

If the viscosity is changed, however, The transfer-functions are not shifted, but merely damped, as expected from the simple one-dimensional analysis outlined above.

Now let us analyse how the model changes with different emitter and collector positions. First, in Figure 3.6 we can see how changing the sampling position affects the transfer-functions. Changing the sampling positions clearly makes non-trivial impact on the system and in addition to shifting some peaks others appear and disappear. However for all sampling positions the resonance frequencies, indicated by the vertical magenta lines in the figure, are present in the system as troughs in the magnitude of the transfer-functions. That they appear as troughs can be

explained by the chosen emitting position of $x_0 = \frac{1}{2}L$, which means that it coincides with a node for all resonance frequencies and since all signals will start from there the waves travelling back and forth in the system will have a perfect phase shift of $n\pi$ everywhere. Since the model has a small attenuation the level will not be perfectly zero, even if they would in a non attenuated system.

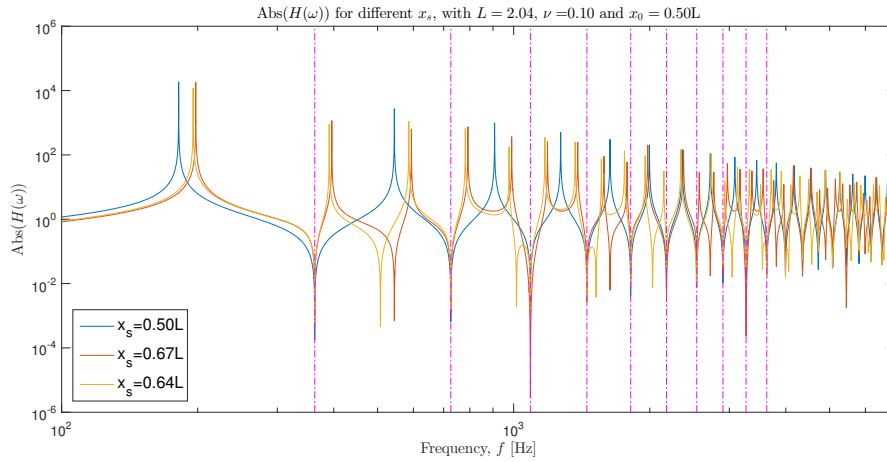


Figure 3.6: Three different transfer-functions for three different sampling positions, x_s , with a fixed emitter position, $x_0 = \frac{1}{2}L$. We can clearly see that the peaks shift slightly with each change and that there are no apparent system to those shifts. The magenta, vertical lines, that indicates the resonance frequencies of the system can however be seen to nicely correspond to troughs in the magnitude of the transfer-functions for all sampling positions.

Changing the emitter's position however does impact this clear connection to the resonance frequencies. This can be seen in Figure 3.7, where only the emitter position of $x_0 = \frac{1}{2}L$ shows all the resonances as troughs. For the other two positions only the resonances that have a node in the emitter position show up as a trough in the magnitude of the transfer-function. For $x_0 = \frac{2}{3}L$ the transfer-function has troughs every third resonance frequency and the transfer-function of $x_0 = \frac{2}{7}L$ has troughs every seventh. In addition to this the transfer-functions have qualitatively very different look and this indicate that the system appear to be very sensitive to the sampling and emitter positions.

Further we can analyse what happens if we keep the sampling and emitter positions at almost the same position along the pipe. The results from the digital waveguide model for this case is shown in Figure 3.8. Here we let the collector's position be at $\frac{2}{7}L$, $\frac{1}{2}L$ and $\frac{2}{3}L$ and the emitter's position is set to $0.9x_s$ in each case. This time all the transfer-functions look quite similar, with the only difference being that some peaks turn to troughs. These troughs seem to be related to the nodes of the frequencies that are present in the system, as can be seen for the $x_s = \frac{1}{2}L$ having troughs in all the resonance frequencies, as in the cases presented above, whereas the other positions only exhibit that every third or seventh resonance, just as before.

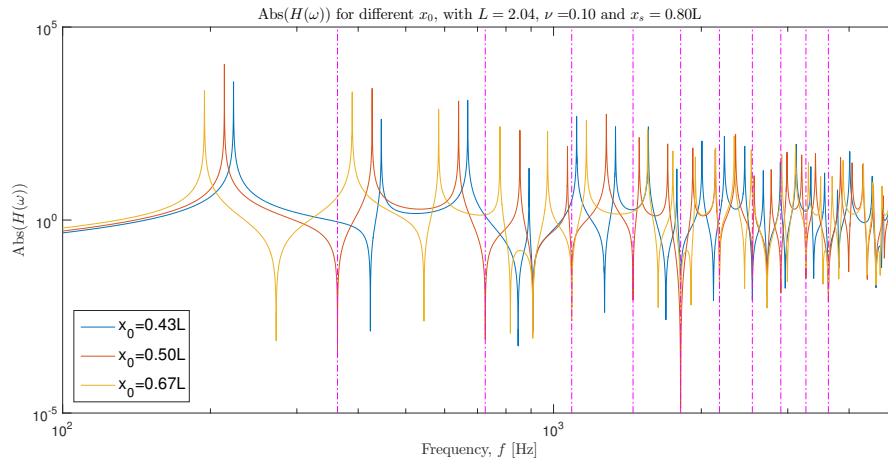


Figure 3.7: The simulated transfer-functions of the digital waveguide model for three different positions of the emitter, $x_0 = \{\frac{3}{7}, \frac{1}{2}, \frac{2}{3}\}L$ and fixed sampling position, $x_s = \frac{4}{5}L$. The theoretical frequencies of the system are indicated as the magenta vertical lines. Again changes in the position affect the transfer-functions in non trivial ways and the resonances also do not clearly appear as troughs in all cases. For each frequency that has a node in the considered emitter position there is however a trough. This can be seen as the yellow line connecting every third trough and the blue transfer-function having a trough at the seventh resonance frequency.

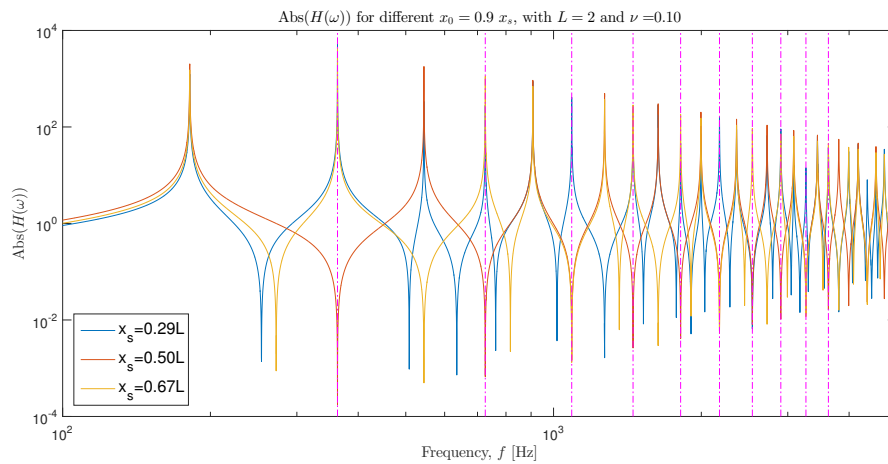


Figure 3.8: The results for the digital waveguide model for three different cases with fixed relative position of the emitter and collector, $x_0 = 0.9x_s$, are presented. The collector positions considered are $\frac{2}{7}L$, $\frac{1}{2}L$ and $\frac{2}{3}L$. The resonance frequencies of the system are indicated as the vertical magenta lines in the figure. We can see that there are similarities between the transfer-functions, but that peaks and troughs appear at different positions in the frequency space. Some peaks can also be seen as troughs in other transfer-functions. The *resonances* are all present in all the transfer-functions, but they appear as troughs if the emitter is placed close to the node of the frequency.

3.3 Frequencies in 3D

To more fully understand how the system might behave we also need to have the three dimensional cylindrical model as reference. As outlined in Appendix A.1, the solution to the viscous wave equation in a cylinder can be found by separation of variables, which in turn means that there are three different numbers that affect the resonances. These are the n^{th} zero of the Bessel functions, the number of angular repetitions, m , and the number of nodes l , in the axial direction along the pipe.

The impact on each of the resonances from changing l is relatively small and looking at the frequencies of consecutive nodes gives us a separation in the order of 10 Hz. Since the first mode will likely be the most prevalent of the z -moderated resonances it might be of primary interest to consider only the frequencies occurring from the modes of the resonating cross sectional *membrane* of the cylinder.

These resonances depend highly (as the ones in z -direction does on the length, L) on the radius of the cylinder. We plug in the radius of the pipe used for further measurements (8.4 cm), as presented in the following sections, and use the sound speed in water 1481 m/s [10]. Then we get that the resonances of the membrane start from 6.7 kHz. In Figure 3.9 the frequencies for the different modes together with the modes themselves are presented.

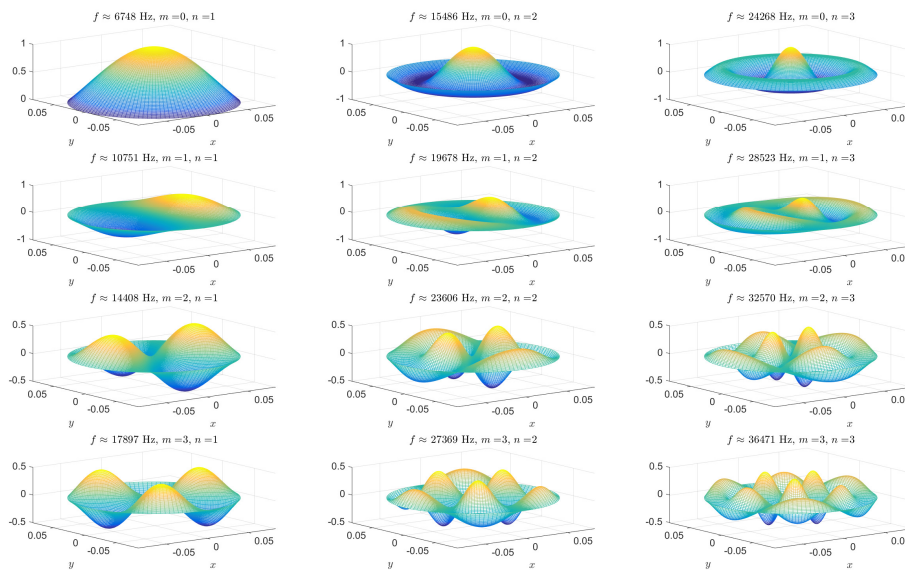


Figure 3.9: The modes the first twelve resonance frequencies of a membrane of radius 8.4 cm *filled* with fresh water at 20 °C. The first frequency of the (0, 1)-mode is approximately 6750 Hz and the other resonance frequencies are given in the sub figure titles of each mode. Only the first five frequencies are below 21 kHz and might thus be detected by the current set up of the Acospector.

4

Experimental setup

HERE, IN THIS CHAPTER, follows an outline of the experimental procedures, including a description of the setup as well as the experimental planning and choices related to the collection of data as well as the experimental design. Ending the chapter is a section on the data processing and analysis techniques used to make sense of the collected data. During the course of making the measurement series new insights into the workings of the system were obtained, which warranted for new measurement series, this evolution of the experiments will also be accounted for in this chapter.

4.1 Materials and setup

For the measurements Acosense's test circuit, a DT7837, was used for data collection and signal broadcasting. On one side of the pipe the force sensor and the emitter were mounted. The force sensor is used to measure the exact signal that is sent into the system and provides a better estimate for calculating the FRF of the system. The signal that is emitted into the system is a multi-sine signal with approximately 11.72 Hz separation starting from zero up to the final frequency at 21 kHz. After the signal has traveled through the system it is collected by an accelerometer placed on the diametrically opposite side from the emitter and force sensor. A schematic picture of this can be seen in Figure 4.1. The pipe is of length 204 cm and has a circumference of 52.5 cm. The sampling at the force sensor and the accelerometer is done at 96 kHz. The time-series signals are subsequently used in order to calculate the CSDs, which in turn are used to form the H_1 -estimate for the transfer-function of the system.

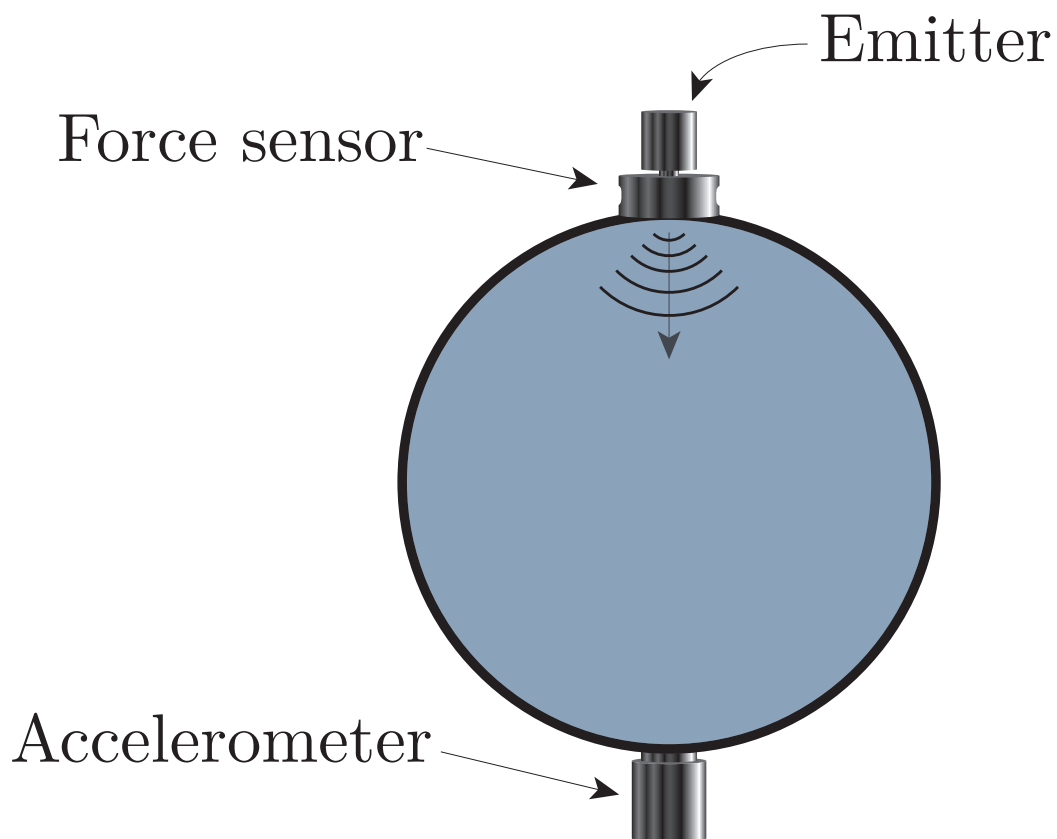


Figure 4.1: Cross section of the pipe with the emitter, force sensor and collector mounted. On one side of the pipe the emitter is connected to the force sensor, which together are mounted on the pipe, and on the diametrically opposite side the accelerometer is mounted.

Before measurements, when filled with water the pipe were allowed to settle at least over night, in order to try to remove unwanted temperature gradients and other factors that might impact the stability of the measurements and thus the results. Due to the construction of the pipe it was kept at an angle from the ground in order to fill it with as much water as possible. However since the taps are placed about a centimeter in on each end, it was inevitable to have a small air pocket in the top of the pipe. In order to minimise the effects of this air pocket the measurement positions were selected such that there was water in the pipe at those positions on the pipe.

To facilitate repeated measures of the different positions on the pipe, pads with external screw threads (fitting for the different sensors) were glued, with Loctite, at a few selected positions along the pipe. These selected positions were chosen such that it would be possible to get the same appearance and disappearance of resonance frequencies as identified in the theoretical analysis described in Section 3. The mounting positions are visualised in Figure 4.2.

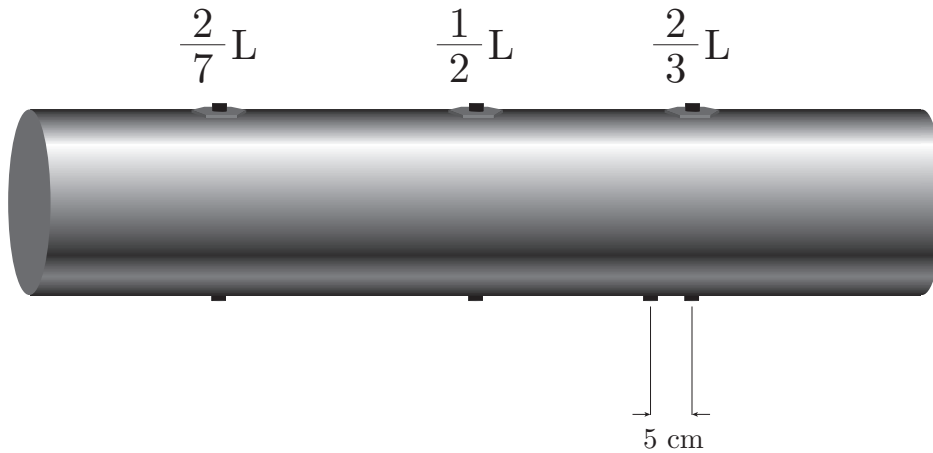


Figure 4.2: The different measurement positions utilised for the measurements are indicated. At each position a pad is mounted on each side of the pipe. In addition to the three pairs of pads at $\frac{2}{7}L$, $\frac{1}{2}L$ and $\frac{2}{3}L$ and extra collection pad was glued at a position five centimeters from the right-most pad.

For the final measurement series on water with different salinity, Acosense’s production glue, *Adraldite 2000+*, was used and two new positions, one in the middle of the pipe and one 60.5 cm in on the pipe, were used.

4.1.1 Parts used

The emitter, a Piezोजना PST1000/10/7VS18 with part number *103194*, was used for all measurements. For the first three measurement days, the force sensor Dytran 1053V2 with part number *464* and the accelerometer Kistler 8703A50M5 with part number *SN 4939433* were used. For the last measurement on water of different salinity, the force sensor with part number *468* and an accelerometer with part number *4939434* were used instead. All components were connected to the DT7837 circuit with their respective cable connections. The time-series signals from both the force sensor as well as the accelerometer were saved to a csv-file and the data was later processed and analysed in MATLAB.

4.2 Experimental design

First, in order to determine the connection to the theoretical digital waveguide model, two measurement series of different absolute and relative positions on a water filled pipe were carried out. Following that was a series that aimed at comparing the effects of different media in the pipe, using water and air as the two media. Later a series measuring a more continuous variation of the media was conducted, where water of different salinity was utilised in order to moderate the density, and thus

the sound speed, of the medium.

In order to minimise unwanted external effects and time variance in the measurements the series were constructed in such a way that measurements were done at each positions three times and the internal order of these repeated measurements were mixed. At each measurement position five samples were collected, in order to reduce unwanted time variations of the system.

4.3 Experimental procedure

As suggested by the circuit manufacturer, the DT7837 was started in advance in order to avoid unpredictable errors. In all the measurements the circuit was turned on the afternoon before the day of the measurements.

At each new measurement position the three components were mounted onto the pads after applying a thin layer of Dow Corning high vacuum grease on the surface connected to the pad (or the force sensor in the case of the emitter). For the initial experiments each component was screwed onto the pad using a moment of 2 Nm, as measured by a torque wrench. With the exception of the emitter that was fastened with a manual wrench. Whereas for the last measurement on salt water the three components were fastened with the torque wrench to 3 Nm with the exception of the accelerometer that was fastened with 2 Nm. After the instruments were mounted, the system was left for at least a minute before any measurements were carried out. This caution was motivated by the desire for reaching a steady state in the system. So, both letting potential vibrations from the mounting subside as well as allowing the emitted sound to fill the system completely. After the one minute of relaxation time five consecutive samples were created, each of which contains 2^{19} measurements of the input and output signals.

4.3.1 Measurement series

For the thesis three different measurement series have been obtained. A short description on each of these follow in the subsequent subsections.

4.3.1.1 Relative and absolute positions in water

This series was collected by observing the spectra from the system at different positions of the emitter and collector. The positions that were considered were the ones shown in Figure 4.2. The absolute positions, i.e., where the emitter and collector were placed at the same position along the pipe, were all measured three times, with ten samples in each position amounting to a total of 30 collected spectra in each measurement position.

In addition to the absolute position measurements, the system was damped with 20 cm wide silicone bands positioned such that the middle and right-most pads

were at $\frac{2}{7}L$ and $\frac{2}{3}L$ in the new shortened pipe, which had an effective length of 89.25 cm. The bands were fastened with metal clasps and were kept in place over the remainder of the measurements. The left-most pad was consequently not used for these measurements. In this setup both absolute and relative positions were investigated and each combination of these was measured three times. The internal order of the measurements were chosen in no particular order, except that repeated measurements at the same position were kept apart in the series. The resulting series of the 18 combination of positions was collected with five spectra in each position, resulting in a total of 15 spectra.

In between the two measurement series, with and without the bands, the top right-most pad fell off and had to be refitted with Loctite to the pipe.

4.3.1.2 Water and air

For the investigation of two different media, namely water and air, the middle and three right-most pads, as indicated in Figure 4.2 were used. Only three of the combination of positions were used, with the emitter placed on the middle, the right-most and the right-most pad, when the collector was placed on the first the right-most and the second right-most pad. The left-most pads were again not used for this investigation. Each position was measured three times each and each measurement consisted of five spectra. First the nine positions were measured for water and later the same series was conducted on the pipe filled with air. Between the measurements on the two media the top middle pad fell off and had to be refastened before the measurements could be continued on air.

This whole procedure was repeated the day after, with the same order of measurements.

4.3.1.3 Varying salinity

To investigate a more continuous variation of the medium water with different levels of salinity was used. This investigation was done through the same procedures as outlined above. As mentioned before the pads were also glued with Adraldite 2000+ glue as opposed to the Loctite glue used in the previous measurements. Ten centimeters on each side from each of the pads 20 cm wide silicone bands were wound two circuits around the pipe, in order to minimise acoustic effects coming from the pipe directly.

The water used was kept in room temperature for the past month and would thus minimise potential effects from temperature gradients. To change the salinity the water in the pipe was pumped out into an external basin to which the salt was added, an addition of half a kilogram for every new measurement point. After the addition of the salt the fluid was pumped back into the pipe and the system was allowed to settle for at least five minutes before any measurements were performed. For salt levels below two kilograms both measurement points were used for every

salinity level. However, after that only the pad positioned at $\frac{1}{2}L$ was used. In every point a series of 36 spectra was collected, each measured with a separation of ten seconds.

4.4 System identification investigation

To investigate the method of parametrising the system with a denominator and a nominator polynomial the pure experimentally obtained spectra were processed through two filters before the system parametrisation algorithm was applied. The first was a simple moving average, where each point in the frequency band is approximated as a mean value out of the seven closest points (including the point itself). After that a band-pass filter was applied. The band-pass used is of order 15 and constructed by using the first order band-pass, given in equation (2.21), to the power of 15. The filtered signal was subsequently used for the system parametrisation.

5

Results

SIDE BY SIDE with the measurement results the model evaluations and potential system characterisations are presented in this chapter, which summarises the results of the thesis. Starting off with presenting the spectra obtained from different system realisations, the results on measurement reliability and the evaluation of the transferability models follow. Finally the results from parametrising the system are presented and the measurements on water with different salinity analysed.

5.1 Relative and absolute positions in water

The first results, presented in Figure 5.1 show how the spectra changes with small changes of the sampling position, x_s , for a fixed emitter position, $x_0 = \frac{1}{2}L$. The spectra are mean spectra over fifteen measurements for each series. It is not clear how to relate the two spectra to each other. Despite the relative proximity of the two sampling points the spectra differ qualitatively in many different ways. First we can conclude that the spectra have no common peaks nor troughs for frequencies above 3 kHz. It is also difficult to deduce any clear effects from potential resonance frequencies, which would be expected to occur with equidistant spacing between peaks or troughs.

Further, in Figure 5.2, the same measurements, but for a different emitter position, $x_0 = \frac{2}{3}L$, are presented.

Next we can look at the effects of changing the emitter's position. These results are presented in Figures 5.3, 5.4 and 5.5, each for different sampling positions. It is again hard to make any direct conclusions from looking at these figures, but one could note that the over all levels of the spectra in Figure 5.3 differ slightly and that this might be explained by the difference in length that the sound has to travel until it reaches the sampling point. This same trend can not be discerned in the

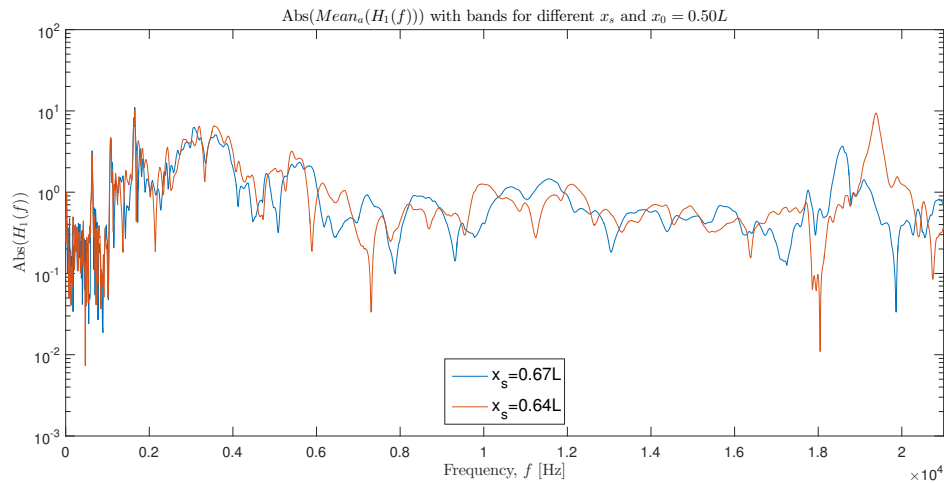


Figure 5.1: The measurements on the water filled pipe with silicone straps fastened. The two series presented are constructed from a total of 15 spectra each and are for two different positions of the accelerometer, $x_s = 0.64L$ and $0.67L$, red and blue respectively.

other two situations, however, even though there are similarities in the qualitative difference between the two series presented in both Figures 5.4 and 5.5.

Finally, we can consider what happens if the positions of both the collector and emitter are changed. The results from this can be seen in Figure 5.6. These measurements were conducted without silicone straps dampening the pipe. The three absolute positions considered were $\frac{2}{7}L$, $\frac{1}{2}L$ and $\frac{2}{3}L$. We can see similarities in the spectra, but also a lot of differences. The two spectra collected at $\frac{1}{2}L$ and $\frac{2}{3}L$ show some global similarities in the level of the spectra, especially when comparing to the third spectra and looking at, for example, the frequencies between 4000 and 9000 Hz. On a local scale the spectra are however all very different.

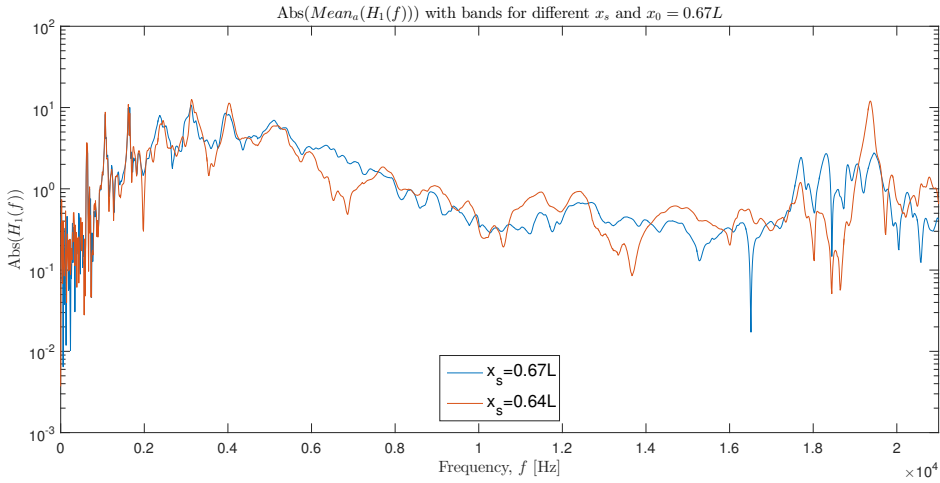


Figure 5.2: Measurements of two different sampling positions, $x_s = 0.64L$ and $0.67L$ the red and blue lines respectively, but with a fixed emitter position, $x_0 = \frac{2}{3}L$. The pipe is damped with silicone bands around the measurement points and the spectra are constructed from a mean over 15 measurements for each position.

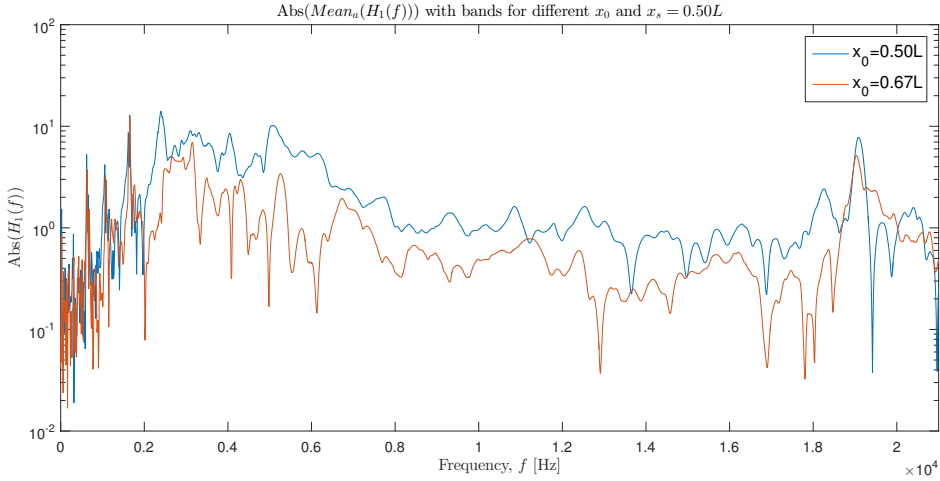


Figure 5.3: Spectra for two different emitter positions, $x_0 = 0.5L$ and $0.67L$ the blue and red lines respectively. The sampling position was kept fixed at $x_s = \frac{1}{2}L$. The spectra are mean spectra obtained from 15 measurements on each position. Two silicone bands were fastened on the pipe during the measurements.

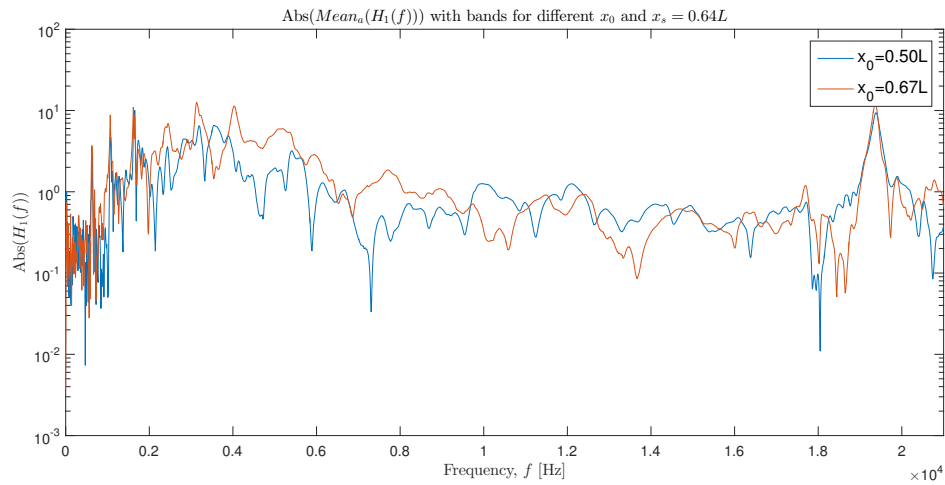


Figure 5.4: Mean spectra for two different emitter positions, but for the same sampling position, $x_s = 0.64L$. The emitter was placed at $0.5L$ and $0.67L$ for the blue and red line respectively. Around the pipe two silicone bands are strapped.

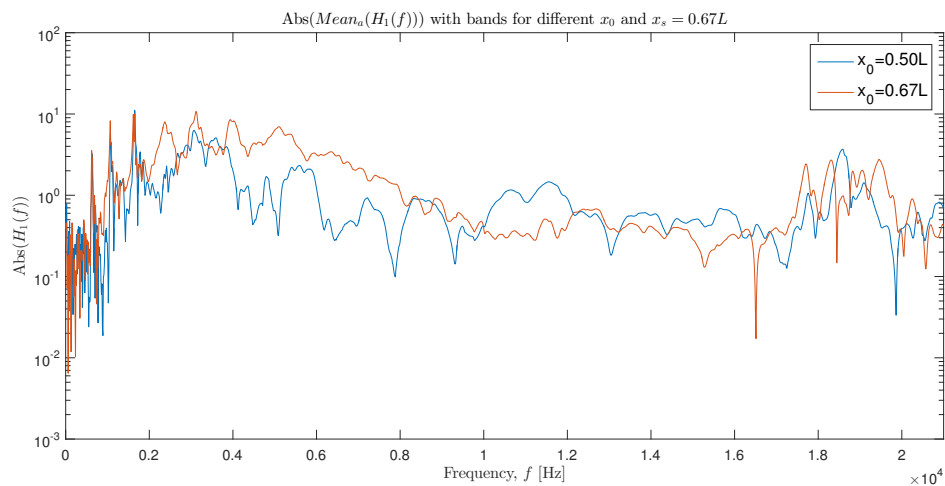


Figure 5.5: Measurements of two different emitter positions, $0.5L$ and $0.67L$. The signal was in both cases collected at $\frac{2}{3}L$. The spectra presented are constructed as the mean out of 15 spectra obtained on measurements in the indicated positions. The pipe was also damped with two silicone bands located on the outside of the measurement zone.

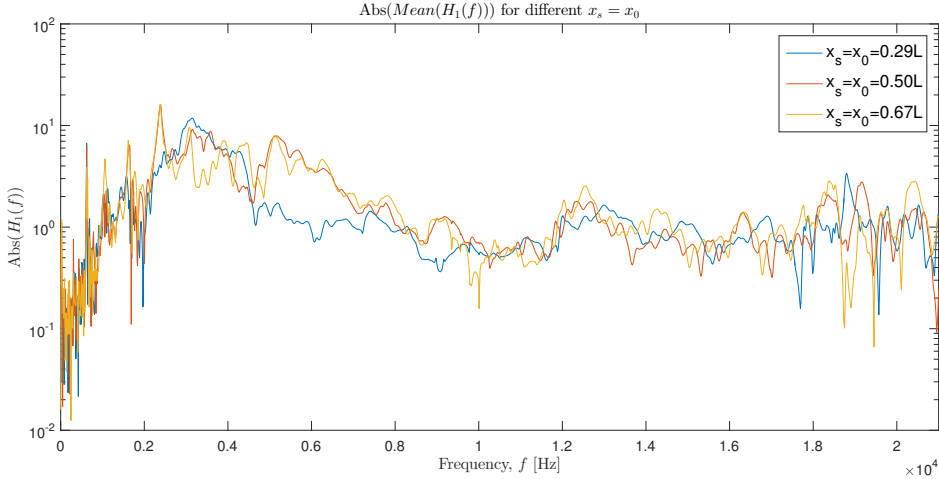


Figure 5.6: Three spectra for different absolute positions of the emitter and collector. The pipe was undamped and the spectra were constructed from taking the mean of 30 measurements in each position.

5.2 With and without silicone bands

Next we can analyse the impact of using silicone bands to damp the sound propagating in the pipe. The results from these measurements can be seen in Figures 5.7 and 5.8 for two different positions of the sampling and emitting positions. The over all level of the spectra is slightly lower with the silicone bands fastened on the pipe, which is especially evident in Figure 5.7. In the second figure this is however not as obvious, where the silicone spectra even dominates the non-damped one at some peaks. For the majority of the frequencies between 8 000 and 18 000 Hz the damped spectra is however at a lower level than the non-damped one. Note the peak standing out at the end of the silicone damped spectra, at around 19 000 Hz. This peak is also discernible in the spectra of the damped pipe presented in Figure 5.7. The frequency of 19 kHz is in the region where the accelerometer is known to be unstable and might thus be an artifact occurring from the components used.

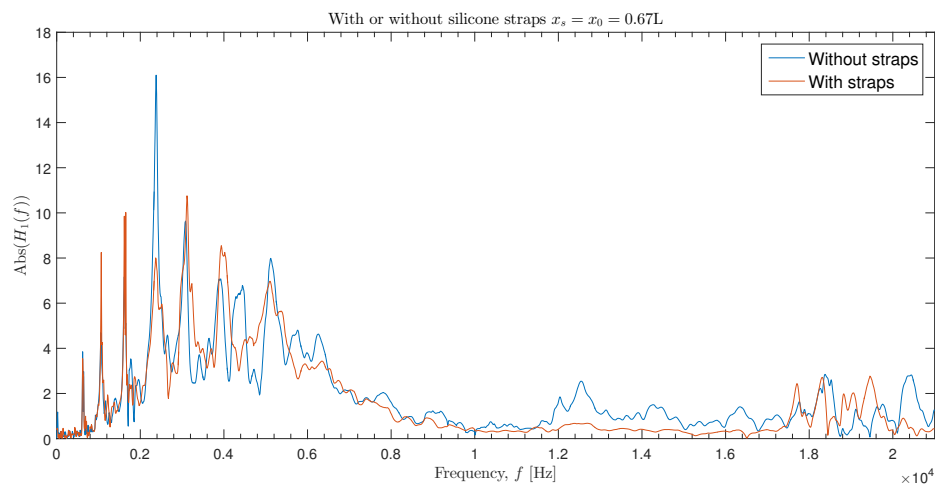


Figure 5.7: Mean spectra of the pipe damped and undamped with silicone bands are presented. The spectra are obtained with the collector and emitter positioned at $\frac{2}{3}L$.

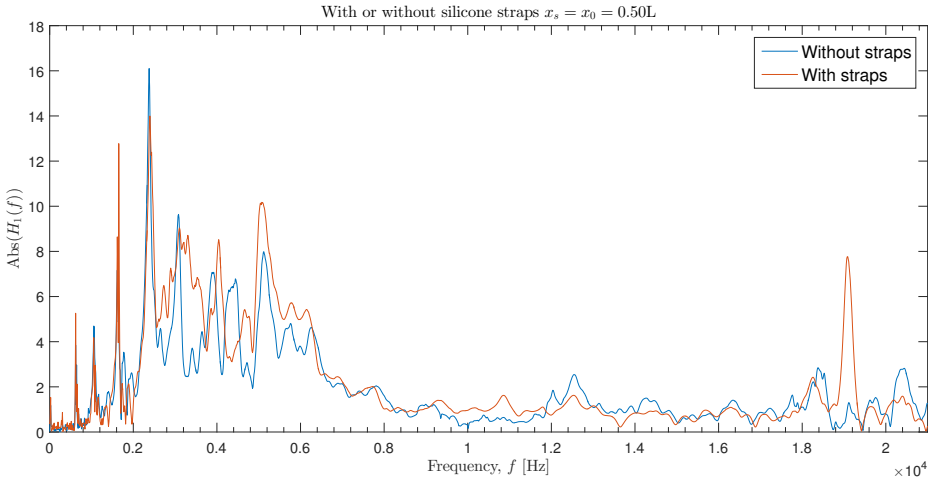


Figure 5.8: Mean spectra of the silicone damped and undamped pipe with emitter and collector placed at $\frac{1}{2}L$. The blue line is without silicone straps whereas the red one is with dampening.

5.3 Water vs. air

To analyse the difference occurring from changes of the medium in the pipe the following figures show the behaviour of the system for water and air for different collector and emitter positions. In Figure 5.9 the spectra of water and air are compared for $x_0 = x_s = \frac{1}{2}L$. The spectra are normalised with the total energy of each spectra respectively, in order to make them comparable. We can see that the spectra from the measurement on air contains a lot of narrow peaks with only a few of any notable amplitude. The water measurement, however, has a smoother character to the spectra with quite a few peaks showing up. There are no clear connections between the two spectra and it is also not evident, despite the normalisation, if any of the peaks present in one of the spectra are related to the ones in the other.

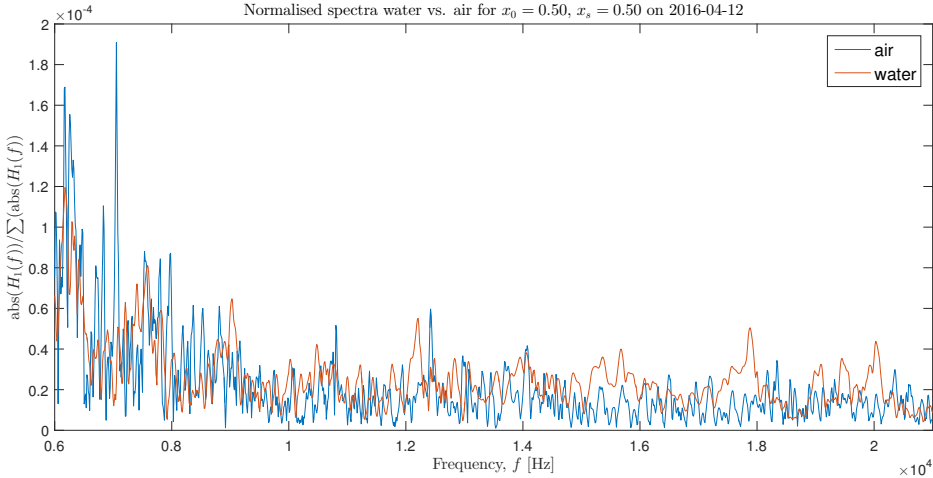


Figure 5.9: Spectra from the pipe filled with water and air, respectively, for $x_s = x_0 = \frac{1}{2}L$. The spectra are normalised with the total energy of the spectra in order to make them more comparable.

In Figures 5.10 and 5.11 the spectra for measurements on water and air for $x_0 = \frac{2}{3}L$, $x_s = 0.64L$ and $x_0 = x_s = \frac{2}{3}L$ respectively are shown. We can again see that the spectra from the air contains a lot of small peaks, whereas the water spectra is somewhat smoother. The over all level of the spectra from the water filled pipe is also lower than the ones from the pipe filled with air.

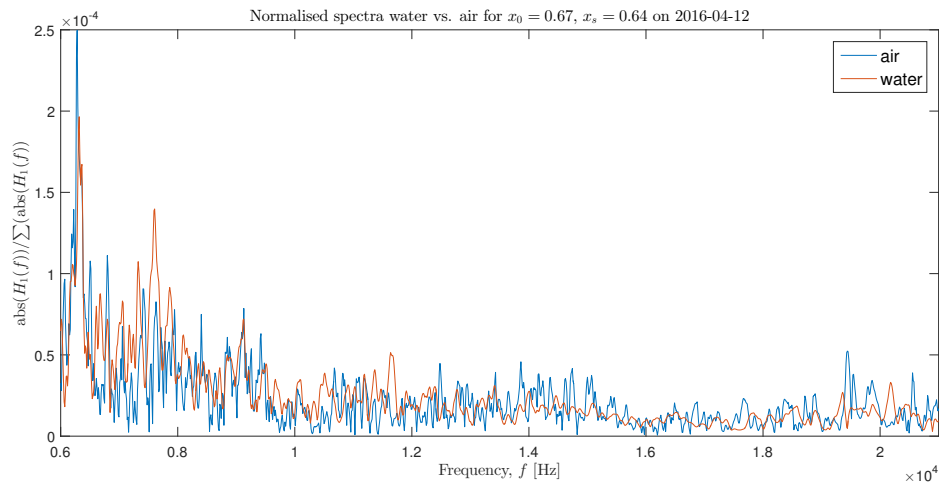


Figure 5.10: Spectra on measurements of the water and air filled pipe, respectively. The emitter was placed in $0.64L$ whereas the collector was at $\frac{2}{3}L$. To make the spectra from the two media more comparable they have been normalised with their total energy.

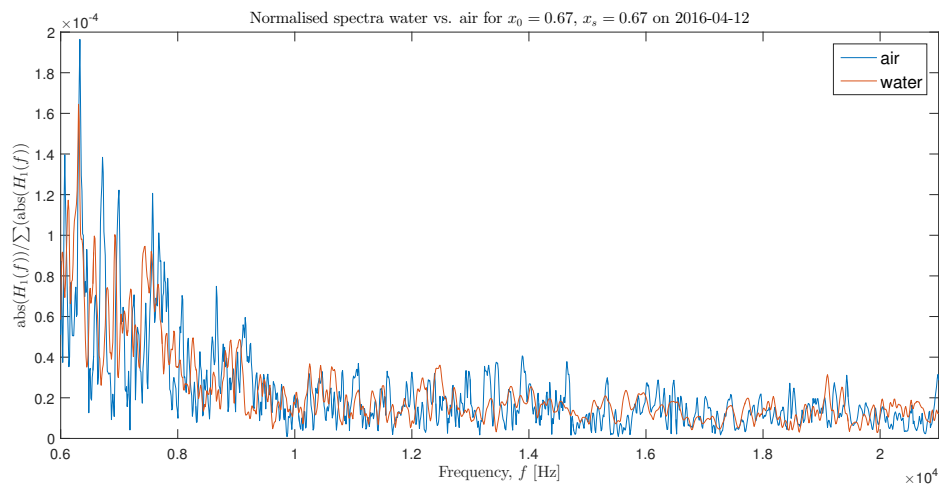


Figure 5.11: The spectra from the measurements on the pipe filled with water and air are shown for $x_s = x_0 = \frac{2}{3}L$. Normalisation of both spectra is done by dividing with the sum of all the amplitudes in the spectra.

5.4 Peak analysis

Figures 5.12 and 5.13 show an empirical fit between consecutive peaks for the spectra obtained on water with both instruments at $\frac{1}{2}L$ and on air with the components at $\frac{2}{3}L$

and $0.64L$ respectively. The peaks are identified through a similar algorithm as the one used in the MATLAB function `findpeaks` and through a visual inspection two peaks were selected in order to try to fit as many consecutive peaks into that pattern as possible. Since resonance frequencies are expected to appear with equidistant spacing between each other this is an empirical approach to find such patterns in the data. For both cases we can see that there is a quite good fit to at least a few consecutive peaks. In the case of water the assumed consecutive peaks does not fall exactly on top of existing peaks in the spectrum, but just off to one side or the other. The spacing between the peaks are 691.4 Hz and 726.6 Hz for the water and air cases respectively.

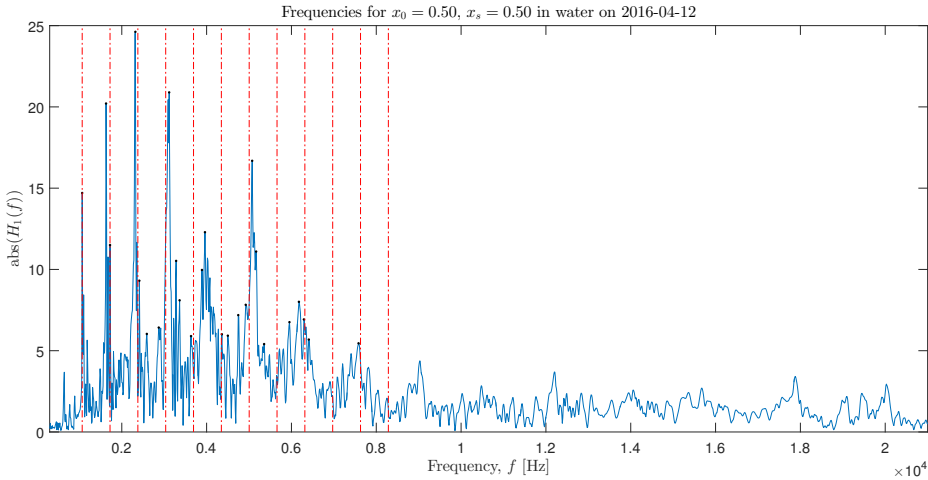


Figure 5.12: Mean spectra for water with the instruments at $\frac{1}{2}L$ is presented together with equidistant spaced vertical lines based on the first and third peak identified in the spectrum. The peak spacing is 691.4 Hz.

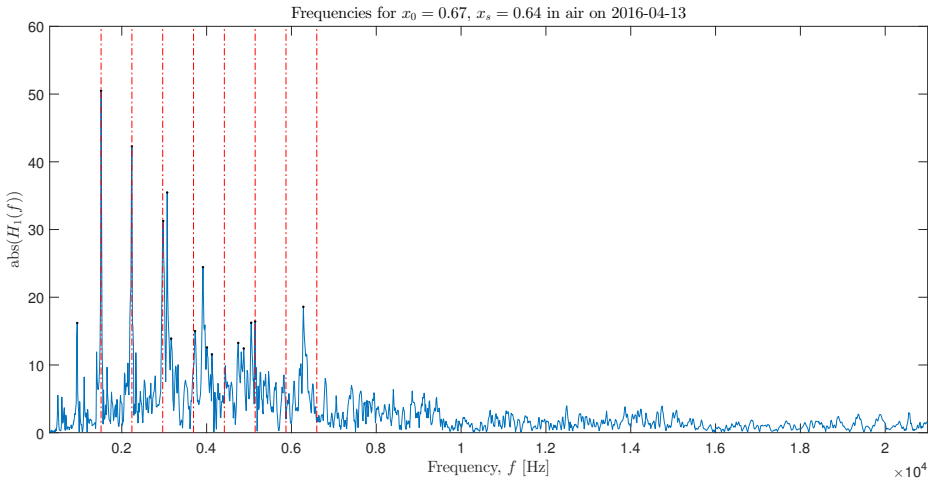


Figure 5.13: The vertical lines are placed with equal spacing starting from the second and third peak identified in the mean spectrum of the air filled pipe with the components placed in $\frac{2}{3}L$ and $0.64L$. The spacing between the peaks is 726.6 Hz.

5.5 Measurement stability

Note that the following evaluation is of the experimental system provided for this thesis and does not accurately represent the system in production by Acosense.

To evaluate the reliability of the results obtained, it is useful to look at the variations that occur between measurements at the same position on the same medium. In Figure 5.14, the mean of the standard deviation within each of the five series obtained in each remounting and each position with the pipe filled with water for all three different positions are presented. We can see that the relative standard deviation is quite high over all, but that it approaches a level of around a few per cent for 2 000 Hz and up. Below this level the relative standard deviation is of the order of 20 % - 200 %.

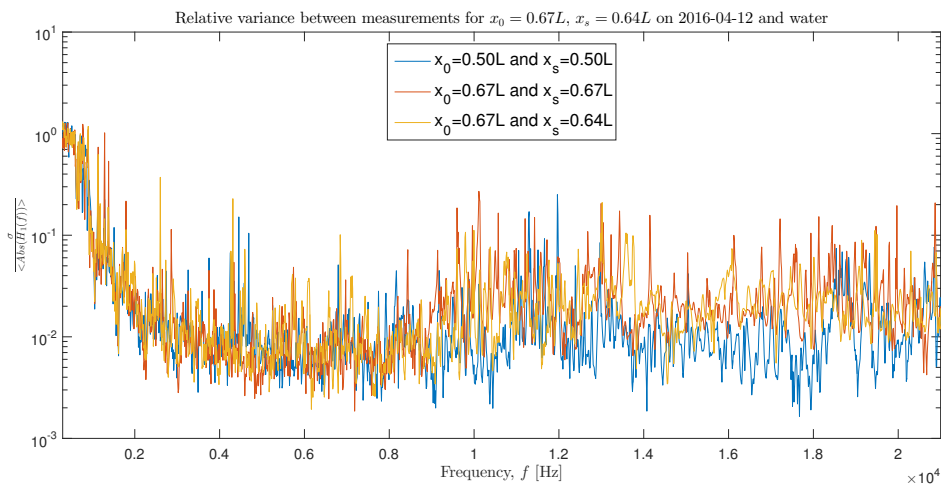


Figure 5.14: Mean of standard deviations calculated from the five measurement series collected in each remounting of the system. These standard deviations are then averaged and collected for each measurement position and each such mean value is presented as a separate line. The standard deviation is related to the spectra amplitude and presented as a relative deviation. The pipe was filled with water and no silicone bands were used to dampen the sound in the metal pipe.

The same analysis for the case of the air filled pipe is presented in Figure 5.15. We can again see a high level of relative standard deviation for low frequencies, but as we approach 2 000 Hz the level is again down to a few per cent. The deviation continues to diminish as the frequency is increased further.

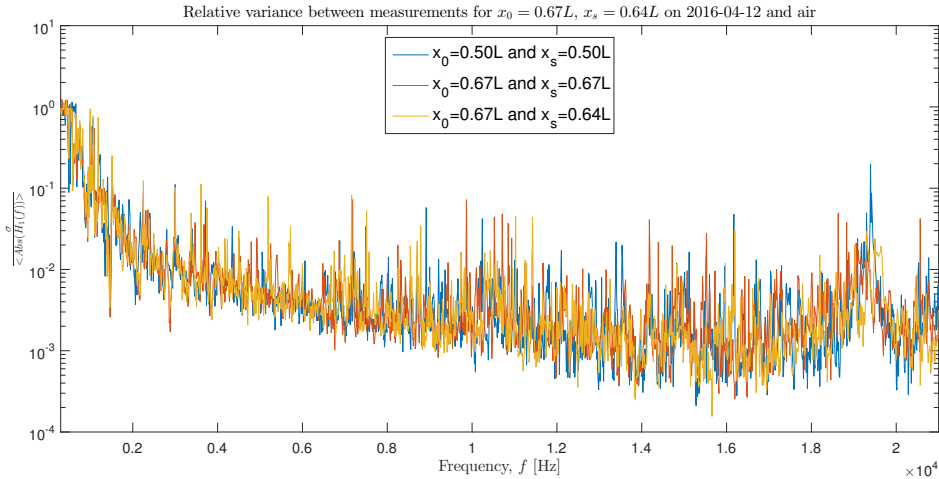


Figure 5.15: Mean standard deviation in relation to the spectra amplitude for the air filled pipe without silicone straps. Each line correspond to the different measurement positions.

5.5.1 Remounting of system

One further check of the consistency of the measurements obtained on the experimental system is to check how much the spectra differ when the measurement components are remounted to the same position. Results from such remounting for the pipe filled with water and air are presented in Figures 5.16 and 5.17 respectively. Here the differences are quite large, with relative errors of 100 %. The error in the water filled system is slightly larger than for the pipe filled with air, but the error levels are still at several per cent even for the part of the spectrum that exhibited low relative variance, as presented in the previous section. From an internal report at Acosense we know that this is not how the production system behaves, but it is an indication of the consistency in the measurements obtained here, on the experimental system.

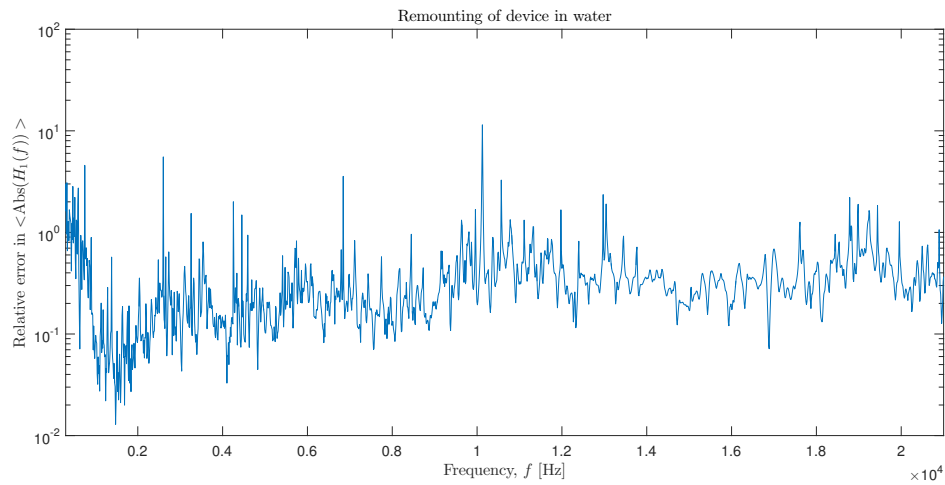


Figure 5.16: Relative error between two spectra before and after remounting the components is presented for the pipe filled with water and without silicone straps. The error is calculated as the absolute difference in amplitude between the two spectra and this difference is later divided with the amplitude of the first spectra in order to get the relative error.

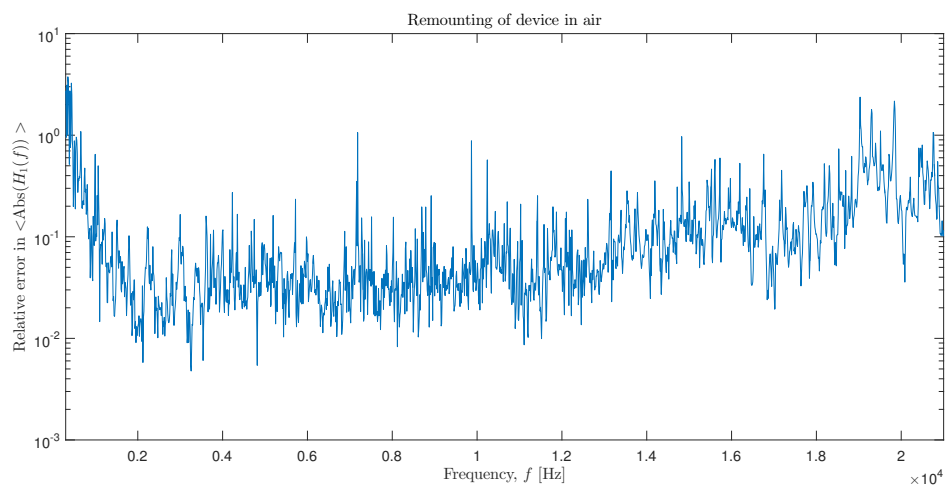


Figure 5.17: The relative error from remounting the components on the system, when filled with air is presented. The relative error is calculated as the difference between the two spectra divided with the amplitude of the first spectrum.

5.6 Evaluation of transferability models

As outlined in the theory section the first order transferability models proposed there have an internal condition that needs to be fulfilled in order for the model to be valid and thus a potential candidate to model the transferability of the system. An evaluation of the models according to these internal conditions follow for the multiplicative and additive models respectively. Concluding the section are the results on the frequency shift model.

5.6.1 Multiplicative model

For the multiplicative model the internal condition is that the fraction between the medium of interest and the reference medium, where both measurements are taken on the same system should equal for all systems. In Figure 5.18 the fraction between two such fractions of different measurement positions (i.e. systems) is presented for water and air as the two media. For the ideal case this fraction should be unity for all frequencies. Together with the pure fraction a linear fit between the two fractions is also presented. The fraction in the new position is assumed to relate to the one in the first position by a linear scaling and a constant according to $\frac{h_1^2}{h_0^2} = c \frac{h_1^1}{h_0^1} + a$. We can clearly see that neither the linear fit of the fraction nor the pure fraction are anywhere close to unity for all the frequencies. The relative fraction is pending between 10^{-2} all the way up to 10^2 . Note however that the linear fitted version seems to mitigate some of the really large peaks, but it is still fluctuating severely.

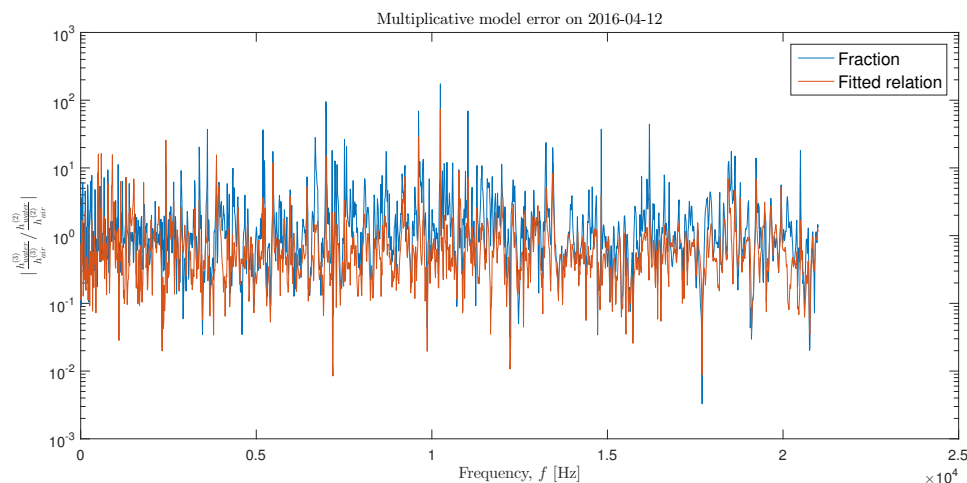


Figure 5.18: Fraction of two measurement positions for the multiplicative transferability model. The blue line presents the pure fraction, whereas the red line is the fraction for the linear fit between the two system realisations. Both lines should ideally be equal to unity for all frequencies.

5.6.2 Additive model

Next, in Figure 5.19, the same comparison for the additive first order model is presented. Again we see that the fractions are far from strictly equal to unity. The over all amplitudes for these fractions are slightly less variable, compared to the multiplicative model.

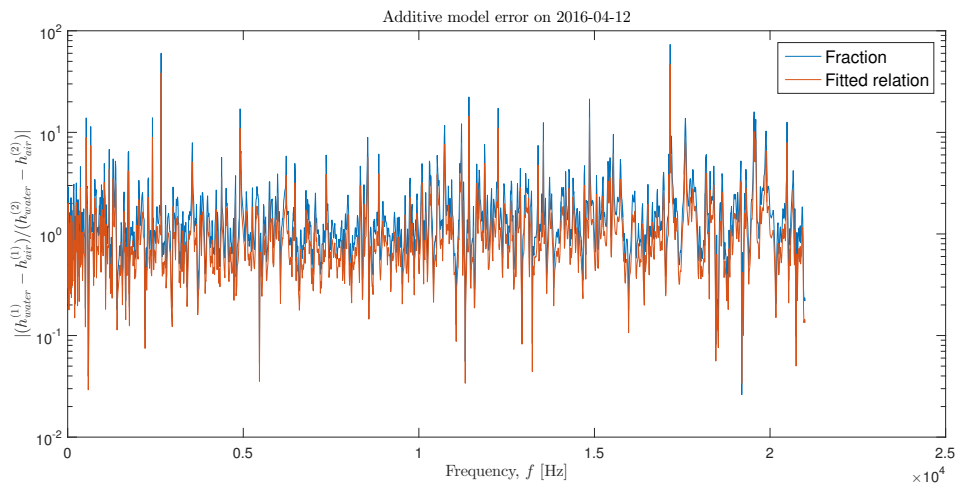


Figure 5.19: Comparison for the additive first order transferability model. A linear fit of the modelling difference is presented as the red line and the pure difference as the blue.

5.6.3 Frequency shift model

The result from the evaluation of the frequency shift model is that it is impossible to relate two spectra with as different character as those of air and water with a pure shift and skew of the spectra. However, due to the failed measurements on salt water together with the time constraint, which meant that the experiments could not be redone, it can not be excluded that it is possible to relate spectra from more closely related media. This initial evaluation however suggest that it will be difficult given that it is fair to expect a shift in both peak frequencies as well as in the relative amplitudes of the peaks and it would thus not be sufficient to only try to make a shift or skew of the spectra in order to relate them.

5.7 System parameter estimation

The results from the parameter estimation of the system on different band filtered transfer-function data and for different polynomial degrees are shown in Figures 5.20, 5.21 and 5.22. For the analysis an arbitrary spectrum obtained during the measurements has been selected to provide an example of how the method might work.

We can see that the parametrisation relatively well approximates the peaks within the band passed areas as well as some of the features outside. Note that the fraction of third degree polynomials very nicely captures the first deep trough in the upper left case of Figure 5.20, whereas the five degree polynomials seem unable to capture this effect, whilst it does capture the consecutive trough and peak instead. The increase of the degree of the polynomials does not seem to affect the features that are captured in any fundamental way and even further increases do not allow the method to capture any more features than the ones presented in Figure 5.21.

For the high end of the spectra the parametrisation seems to run into some issues with the approximation of the features, as seen in Figure 5.22. There is a lot of peaks present even in the small band passed intervals which seem to decrease the performance of the method. Note the degree to which peaks outside the band passed interval is picked up, several thousand hertz outside the applicable interval, which is especially interesting considering the high-order band pass filter that moderates the fit of the signal (order 15).

To evaluate the accuracy of the optimisation method to acquire the parametrisation we might look at only the part of the signal that falls in the selected band. The results from that are presented in Figure 5.23. We can see that the peaks are captured quite accurately by the polynomials, when no consideration is put into fitting the signal outside the current frequency band. Note the high degree of similarity for the two plots to the right in the figure, whereas the two bands presented to the left seem to include features that are difficult to capture with the system identification. Further increases of the order of the polynomials used does not help in capturing these features present in the two left cases.

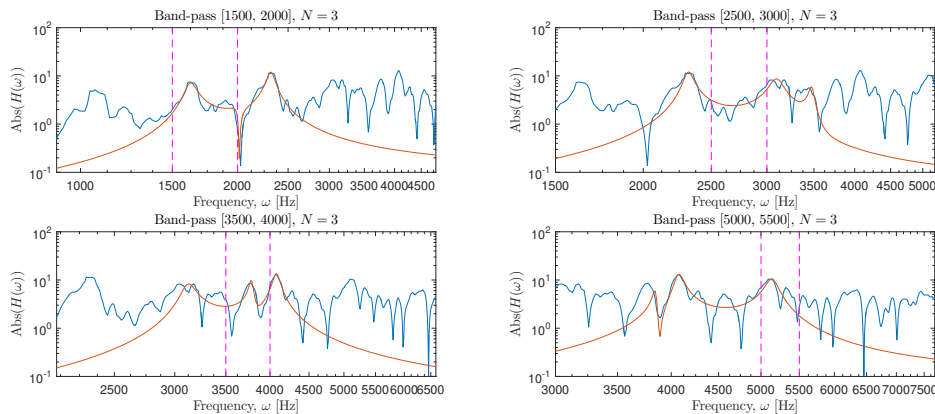


Figure 5.20: System identification on four different band passes with frequencies 1500-2000, 2500-3000, 3500-4000 and 5000-5500 Hz, as indicated in the subplot titles and as the vertical lines. The polynomial in denominator and nominator are both of degree three.

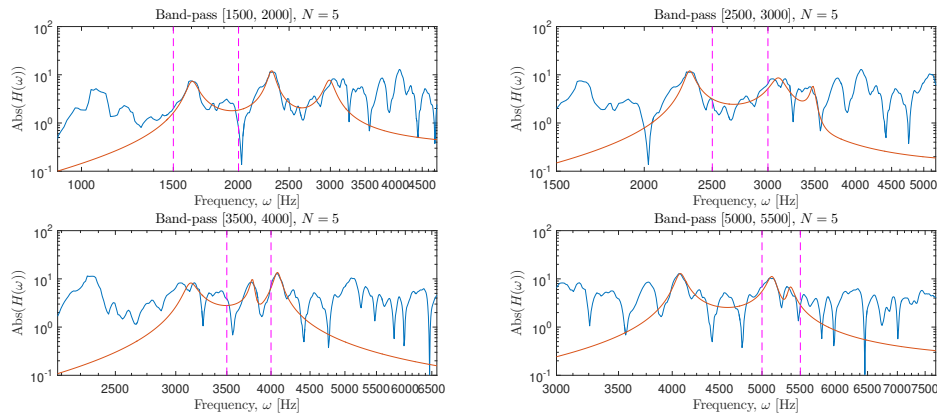


Figure 5.21: Here the system identification is done for the fraction of two five degree polynomials in different band passed frequencies, as indicated in the title of the sub figures and according to the dashed vertical lines in the figures.

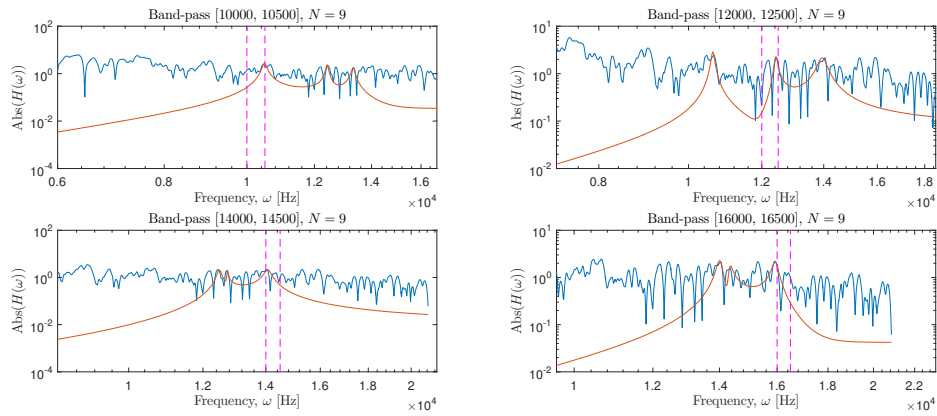


Figure 5.22: Four different band pass filters applied to the signal before the system is parametrised with two nine-degree polynomials. The frequencies considered are between 10 000 and 16 500 Hz. The band passed frequencies are indicated as dashed vertical lines and are also given in the sub plot titles.

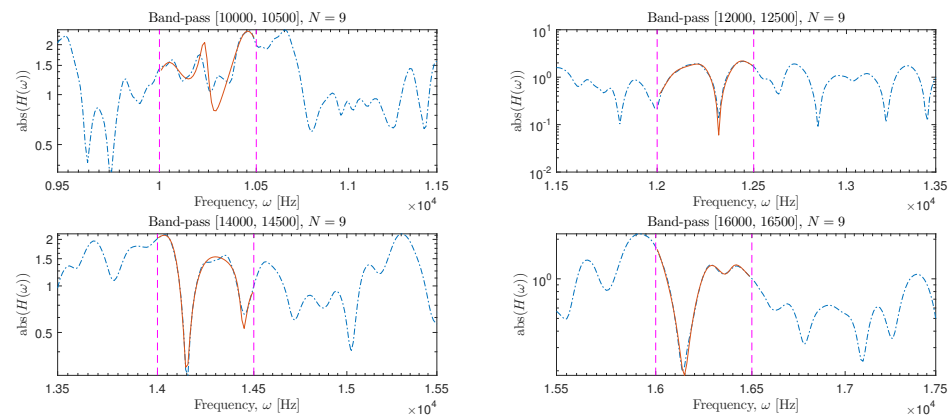


Figure 5.23: System identification algorithm used on the only the part of the signal that fall into the bands shown in the sub figure titles as well as indicated through the vertical magenta lines in each plot. The polynomials used in the system parametrisation are both of order $n = 9$.

5.8 Measurements on salt water

The salt water measurements can reasonably be discarded due to some unknown failure during the experiments. As shown in Figure 5.24 the relative standard deviation in the measurements of water with different salt levels is of the magnitude of 10 % over the whole spectra and the spectra also seem to drift between consecutive measurements on the same setup, as can be seen in Figure 5.25. The two arrows in the figure indicate how the spectra change over the consecutive measurements. Despite the seemingly small deviations in the peaks between 2000 and 4000 Hz, the relative standard deviation is actually still in the magnitude of around 10 %, as can be seen in Figure 5.24. The deviations appear smaller due to the log scale on the y -axis. When comparing the drift between the different setups there does not seem to exist any clear correlation between how the spectra change with time.

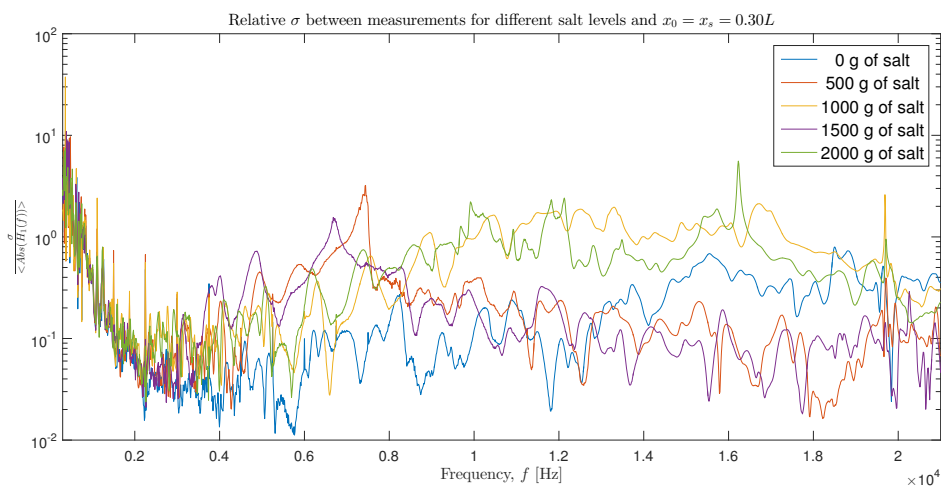


Figure 5.24: Relative standard deviations for the spectra obtained from 36 consecutive measurements during which no changes were made to the system. Each presented line correspond to this relative standard deviation for different amount of salt dissolved in the water. The emitter and collector were both placed 60.5 cm in on the pipe, with a 20 cm wide silicone strap on each side of that position.

If we further split the analysed signals into its components and look at the PSDs for the force sensor and accelerometer signals respectively we can see that the drift seems to primarily occur in the accelerometer signal, whereas the force sensor is reasonably consistent over the course of the measurements.

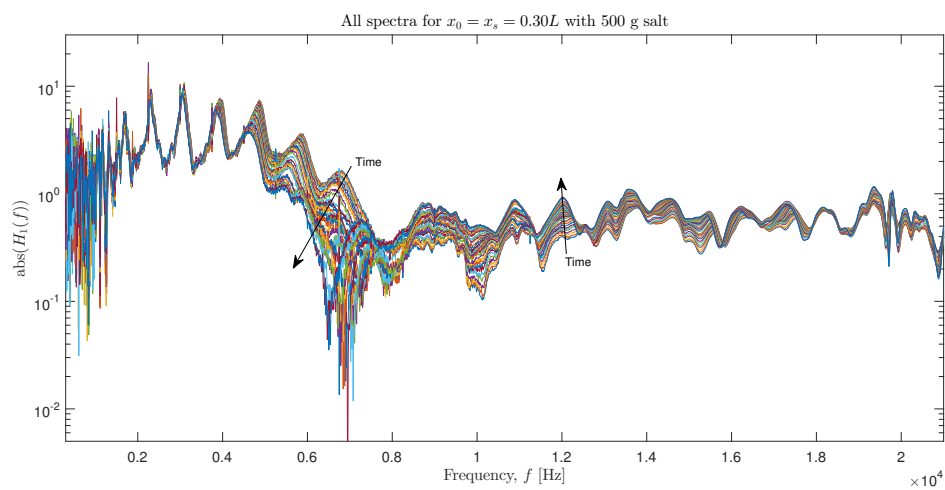


Figure 5.25: The arrows indicate how the spectra change over consecutive measurements on water with 500 g salt dissolved and where the emitter and collector both were placed 60.5 cm in on the pipe, with 20 cm wide silicone straps on each side of that position.

6

Discussion

AS WITH MOST PROJECTS this thesis has indeed had some challenges and these together with the results of the theoretical investigation, the measurements and a comparison between the two are discussed in this chapter. Additionally a section on possible future work is presented, including possible ways forward towards determining the transferability of the system.

6.1 Transferability models

Based on the results from this thesis it is possible to infer that the transferability of the system needs to be modelled through non-linear models. However, due to the lack of measurement data it has not been possible to investigate such models. The imposed restrictions on the number of setup measurements at new (re)installations of the systems further imply that such high order models are of no practical use, since they would effectively need several measurement on several different media of controlled qualities. Not only do these media samples need to be equivalent to the samples used in the first setup, but they should ideally also span and encompass the possible medium variations for the production system. The result being that the effective calibration time and effort would not be reduced by any significant amount even if it were possible to find a transferability model.

It could further be concluded that the first order models as well as the composite models, of the first order, is far from sufficient to capture the complexity of the system. The conditions imposed from the model equations are far from fulfilled in both of the linear cases. For the composite model it can be concluded, given the analysis of the model together with the acquired understanding about the system, that it would be insufficient to model all aspects of the spectra. Additionally it will be very difficult to find an optimal composite function that would relate the spectra from the different media, since the change of medium is expected to result in both

frequency shifts as well as amplitude moderations.

6.2 Comparison to theory

The main idea of the set up of the thesis was to start from a thorough theoretical model, use that to construct reasonable experiments and then relate the results to the models. However, due to lack of variable experiment parameters and the internal fluctuations between experiments and the low reproducibility of measurements on the accessible system this comparison gradually slipped more and more out of reach for the project. After analysing the obtained spectra for potential resonance effects, both from the ideal one dimensional model, the viscous one and three dimensional models as well as the waveguide it was impossible to find any concrete similarities between the results and the theoretical models. This lack of similarities may be due to several reasons. Firstly it might be an issue with an actual misalignment between the chosen model and the system which then obviously would lead to dissimilar results. The modelling parameters could have been chosen poorly and would thus not capture the real effects in the system or the choice of looking at the resonances of the system might not at all pose the right assumptions in order to carry out the right type of analyses and data processing.

Secondly, it might be due to the collective complexity of the models as well as the system itself and that this complexity in practise means that the results are close to impossible to relate to each other due to all effects that are present, even though they might in fact be similar. This is something that we saw not the least in the digital waveguide model, for different sampling positions. Really small changes seemed to induce very intricate changes to the system and if that model resembles the real system in any way there might be really small changes pushing the system outside the boundary for where the theoretical model would be applicable and thus render it impossible to run a comparison.

Thirdly, the general idea of following the resonance frequencies might not be at fault in itself, but there might be overlaid effects that remove the clear connection to these effects and other parts of the system might well play an equally important part as the resonances and trying to discern these from the seemingly quite flat spectrum is thus not as trivial a task as one would have hoped for.

Some spectra do indeed contain almost equidistant peaks at least for a few consecutive peaks, as seen in Figures 5.12 and 5.13. It is however dubious if these peaks are indeed springing from the same resonance phenomenon or if they just happen to be placed *almost* equidistantly. For the case of the water there is not even a perfect alignment between the peaks and the proposed equidistant spacing. It might be possible that the peaks are indeed from some system effect, but since there is no clear reproducibility between different measurement positions and not even between the same position on different days it is hard to say in what way these peaks would be related to the system. Further the spacing does not seem to have any direct link to the separation found in any of the theoretical models. Not only does it differ

highly between the different measurement series, but it is also not even close to the numbers obtained from the theoretical models' resonance frequencies.

The idea with the measurements on salt water was to get a continuous change in the medium parameter and thus be able to validate or reject the hypothesis that some media parameters do change the spectra by shifting the peaks according to the change to the sound propagation speed, or some other medium parameter. However, due to poor measurement results and stability (see the following section for a discussion on that) it was impossible to clearly reject or accept that hypothesis.

6.3 Measurement reliability

From the analyses on the stability and variance in the measurements on the experimental system it can be assumed that similar systems are susceptible to changes in surrounding parameters, including the mounting procedure as well as the stability of the medium and pipe themselves and that care should be taken when installing the components and setting up the system to minimise such effects. The positive thing with having a system that is sensitive is that it is fair to assume that given the right setup it should be possible to capture quite subtle changes in the medium, which is what we want to measure, but the downside is obviously that external variations and noise also are picked up and destroy the measurements. With the lack of controllable aspects for our experimental investigations these external factors together with possible unknown ones seem to have impacted to such an extent that they rendered measurements of poor quality, especially the ones on the salt water. For most of the measurements however the large qualitative aspects seem to remain between the different spectra and in those cases the results are still applicable for further analysis as the one outlined in the previous chapter.

6.3.1 Sources of error

What might be the reasons for the errors or noise that are present in the measurements? There are several potential sources. First, the pure setup of the pipe and the procedure when mounting and remounting the components introduce potential changes to the system, which we can see is also susceptible to those changes, as seen in Figures 5.16 and 5.17, where the remounting of the device is analysed. The silicone bands do also affect the obtained spectra, at some places of the spectra with large impact, where complete segments are damped away or brought forward, whereas in other areas they only seem to moderate the amplitude of the large peaks. A more thorough investigation into how external objects in contact with the pipe affect the obtained spectra seem to be warranted, unless one can ensure that no such effects will occur during measurement series or in production. For the measurements collected for this thesis all measurement series have been supposed to be internally consistent, but they were never supposed to be used for cross comparisons and it is thus hard to use them as a way of determining the factors, which might

be the cause of the differences seen in the spectra from the different measurement dates. The human factor, the pipe used as well as the positioning of the pipe, in a horizontal orientation on movable bases supporting the pipe, are also large potential factors of errors, especially considering the inconsistencies in between the measurement series.

Further sources of noise or error are changes in uncontrollable parameters, such as temperature and air pressure. Looking at the measurements on the salt water it seems to be more drift in the output signal at the accelerometer compared to the input signal at the force sensor. The day of the measurements was a very hot day and it is possible that the temperature of the room itself has such an impact that these drifts occurred. However, the drift is not limited to the accelerometer channel, so temperature differences, which moderate the pipe and system, can not be the only factor that affected the system. If the components themselves are susceptible to changes in temperature that might explain that there is a change in the force sensor as well. Else there might be any number of unforeseen effects that moderate and induce the drift of the system. Since the new system with the production glue was used for these measurements it is fair to assume that it is not due to a physical drift of the components. The most likely explanation is a loose contact of the accelerometer or that the specific mounting induced a particular instability of this experimental system.

In addition to the physical instruments there might be errors occurring from the digital processing of the signal as it has been collected. As outlined in the theory section it is the H1-estimate that is used in order to estimate the transfer function of the system. This is based on the assumption that the error can be reduced by assuming that the error at the output is uncorrelated with the input. Since the new instruments use a force sensor to measure the input this assumption is not 100 % true anymore. The force sensor itself should only collect the signal from one specific direction with a close proximity and external noise should thus not affect too much. But, if environmental noise is picked up at the force sensor it will directly be part of the H1-estimate and the assumption that the error is minimised is not longer true. This is however something that needs to be investigated further for any conclusions to be made with whether this is an issue or not, but it might potentially be a source of errors to the measurements presented here. This is however not something that has been verified in the investigation done throughout this thesis.

6.4 Information contained in the spectra

Based on all the measurements and the stability over the spectra over all these collected samples it seems reasonable to conclude that one should cut the spectra at around a few thousand hertz and only consider the spectra for higher frequencies. Looking at the analysis of the relative standard deviation for water and air, as presented in Figures 5.14 and 5.15, this cutoff frequency should probably be selected to around 3 000 to 4 000 Hz, where the standard deviation varies with around a

few per cent rather than 10-20% as is the case for the lower frequencies. Discarding some of the lower frequencies is also something that is advocated by Acosense.

6.5 Future work

Based on the investigation throughout this thesis some interesting questions and areas have arisen and in the following sections some of these will be outlined as a suggestion for future work in order to improve and optimise the use of the Acospector and similar instruments.

6.5.1 Transferability

With access to high quality data from several sources and where the medium has been changed more or less continuously over the measurements it would be possible to make a final verdict regarding what would be needed to model the transferability of the system. However, given the current investigation it seems highly unlikely that such a model would be of use in practise since it would need several reference measurements and it would thus defeat the purpose of reducing the installation and calibration time of the system. Other uses of the system, i.e. through sending other signals or having a more complex setup of several sources and collector positions might provide new ways of finding a transferability of the system. In conducting such an investigation considerations should be made with respect to the potential trade-offs in terms of added complexity of mounting the device, the practical use of the system and the final value added from achieving the transferability.

6.5.2 Investigate alternative uses for the instrument

Currently the active acoustic spectroscopy system is used by emitting a broad band signal consisting of a specified multi-sine signal with a separation of 11.72 Hz. This signal is emitted continuously and it is assumed that a steady state is reached, which is the basis of the measurements. However, there are several other possible signals to use to probe the system. Some alternatives are to send out and sample in impulses, which would allow for extraction of specific frequency components as well as stripping of unwanted effects if the signal is further windowed on the sampling side. Since the propagation speed differs through different media a measurement of the response for different sampling delay might give completely new information about the system. Yet another possible signal is to let it sweep through the frequency band of choice rather than emitting all frequencies at once. There are a lot of possible aspects to investigate here, but they should all come secondary to creating an understanding of how the system really works in detail. With that knowledge it would then be feasible to make an informed decision of which signal that is most appropriate for the application at hand. After the investigations from the thesis

it feels as if there is a lot of undiscovered potential in the system, given that the sensitivity issues to external noise is solved.

6.5.3 Develop alternative models for feature extraction

Together with changes to the way of measuring it is also possible to further investigate the different ways of extracting features from the spectra that is obtained. Given the theoretical investigations of this thesis it seems likely that many potential effects would come in through shifts to the peaks and troughs that appear in the spectra. It would thus make sense to devise a model that captures those effects and not only consider the spectra frequency by frequency as it is done today.

6.5.3.1 System parametrisation

One potential way of doing this is through the system parametrisation presented in this thesis. By estimating the spectra in several small frequency bands the coefficients of the estimation polynomials might be used as a way of comparing different spectra. Such an abstraction of the spectra would also capture the shifts in both amplitude and position of the peaks as well as the troughs. To implement this model a more stable optimisation of the polynomial fitting should however be used and the data should ideally be scaled appropriately in order to remove issues with large numbers and zeros in the nominator and denominator polynomials, resulting from the large values of the frequencies used. Similar methods, which would result in similar characterisation of the system would be to use pure polynomial approximations, splines or moving averages in order to smooth the spectra. These last suggestions however imply a very different assumption regarding the system, namely that the frequencies are not independent of each other, such that adjacent frequencies affect each other. Only in such a regime would it make sense to create a moving average or such approximation of the spectra. This assumption of frequency independence is the one which the current mode of analysis hinges on and applying a moving average to the spectra would thus not only violate that assumption but also remove or even destroy data. So, in order to use that way of characterising the data one should make sure that no information is lost in the process.

6.5.3.2 Peak identification and tracking

Other ways of characterising the spectra is by identifying and tracking the peaks and troughs of the spectra. Potentially interesting properties here include the frequency of the peak, peak center, width as well as relative amplitude compared to the other peaks in the spectra. Tracking changes to these characteristics of the peaks might very well prove to be a very information rewarding activity. This however is based on the assumption that it is changes to the peaks of the spectra that contains the information about the system. Note that this is basically a reduced version of the

system parametrisation, which would also capture this information in the coefficients of the nominator and denominator polynomials.

6.5.4 Relating the features to changes in the medium

In addition to the PLS and PCA models used currently to associate changes in the spectra with changes in the medium parameters it would be interesting to investigate the possibility of using models such as Hidden Markov Models or possibly other machine learning techniques, including Artificial Neural Networks and Support Vector Machines in order to maximise the potential of the extracted features.

7

Conclusions

BASED ON THE INVESTIGATION made throughout this thesis it can be concluded that first order linear multiplicative and additive models are insufficient to capture the transferability of the system. Due to the complexity of the spectra and the high number of different effects resulting from changes of the media the proposed composite transferability model could also be rejected as too simplistic. Further expansions of the models would result in an increased need for initial reference measurements, which would, to a large extent, defeat the purpose of reducing the calibration time at new installations. That said it can not be ruled out, given specific media or other uses of the system, that there might still be possible to find a suitable model capturing the transferability of the active acoustic spectroscopy system. Before any further such investigations are carried out the focus should however be put to finding the main parameters that affect and impact the measurements from the system. This is needed in order to narrow down the features that might be of interest in the final results as well as to minimise the occurrence of errors. Based on the performed measurements it could be concluded that the experimental system is highly sensitive to basically all changes to environmental as well as system parameters and that it could thus be considered unfit for further experimental uses. Determining the robustness of the system with respect to these parameters and setting up a controlled test environment should be the main focuses before any future work on the transferability is conducted.

Bibliography

- [1] Aarts, R. (2011). System identification and parameter estimation. https://www.utwente.nl/ctw/wa/web_dev/old/lectures/113170/notes/notes.pdf. [Online; accessed 28-April-2016].
- [2] Acosense (2013a). About acosense - who we are. <http://www.acosense.com/en/about-2/>. [Online; accessed 19-January-2016].
- [3] Acosense (2013b). Industries. <http://www.acosense.com/en/industries/>. [Online; accessed 19-January-2016].
- [4] Alba, F., Crawley, G., Fatkin, J., Higgs, D., and Kippax, P. (1999). Acoustic spectroscopy as a technique for the particle sizing of high concentration colloids, emulsions and suspensions. *Colloids and Surfaces A: Physicochemical and Engineering Aspects*, 153(1–3):495 – 502.
- [5] Allegra, J. and Hawley, S. (1972). Attenuation of sound in suspensions and emulsions: theory and experiments. *The Journal of the Acoustical Society of America*, 51(5B):1545–1564.
- [6] Babick, F., Hinze, F., and Ripperger, S. (2000). Dependence of ultrasonic attenuation on the material properties. *Colloids and Surfaces A: Physicochemical and Engineering Aspects*, 172(1):33–46.
- [7] Bensa, J., Bilbao, S., Kronland-Martinet, R., and Smith III, J. O. (2003). The simulation of piano string vibration: From physical models to finite difference schemes and digital waveguides. *The Journal of the Acoustical Society of America*, 114(2):1095–1107.
- [8] Dukhin, A. S. and Goetz, P. J. (1996). Acoustic spectroscopy for concentrated polydisperse colloids with high density contrast. *Langmuir*, 12(21):4987–4997.
- [9] Dukhin, A. S. and Goetz, P. J. (2001). Acoustic and electroacoustic spectroscopy for characterizing concentrated dispersions and emulsions. *Advances in Colloid and Interface Science*, 92(1):73–132.
- [10] Engineering-toolbox (2016). Water and speed of sound. http://www.engineeringtoolbox.com/sound-speed-water-d_598.html. [Online; accessed 25-April-2016].

- [11] Epstein, P. S. and Carhart, R. R. (1953). The absorption of sound in suspensions and emulsions. i. water fog in air. *The Journal of the Acoustical Society of America*, 25(3):553–565.
- [12] Esbensen, K. H., Halstensen, M., Lied, T. T., Saudland, A., Svalestuen, J., de Silva, S., and Hope, B. (1998). Acoustic chemometrics—from noise to information. *Chemometrics and Intelligent Laboratory Systems*, 44(1):61–76.
- [13] Esbensen, K. H., Hope, B., Lied, T. T., Halstensen, M., Gravermoen, T., and Sundberg, K. (1999). Acoustic chemometrics for fluid flow quantifications—ii: A small constriction will go a long way. *Journal of Chemometrics*, 13(3-4):209–236.
- [14] Folland, G. B. (1992). *Fourier Analysis and Its Applications*, volume 4. American Mathematical Society, Providence, Rhode Island.
- [15] Inam, M. A. and Frances, C. (2010). Effects of impurities on particle sizing by acoustic attenuation spectroscopy. *Powder Technology*, 201(1):21–26.
- [16] Jaeger, R. C. and Blalock, T. N. (2010). *MICROELECTRONIC CIRCUIT DESIGN*, volume 4. McGraw-Hill, New York, NY 10020.
- [17] le Rond d’Alembert, J. (1747). Investigation of the curve formed by a vibrating string. *Acoustics: Historical and Philosophical Development*, pages 119–123.
- [18] Levine, H. and Schwinger, J. (1948). On the radiation of sound from an unflanged circular pipe. *Physical review*, 73(4):383.
- [19] Liljenberg, T., Backa, S., Thegel, L., and Abom, M. (2002). Active acoustic spectroscopy. Patent no. PCT/SE01/01565.
- [20] Merriam-Webster (2015). Sound. <http://www.merriam-webster.com/dictionary/sound>. [Online; accessed 26-January-2016].
- [21] National-Instruments (2008). Fft fundamentals. http://zone.ni.com/reference/en-XX/help/372416B-01/svtconcepts/fft_funda/. [Online; accessed 29-January-2016].
- [22] Råde, L. and Westergren, B. (2004). *Mathematics Handbook for Science and Engineering*, volume 5:9. Studentlitteratur AB, Lund.
- [23] Rocklin, G. T., Crowley, J., and Vold, H. (1985). A comparison of h1, h2, and hv frequency response functions. In *Proceedings of the 3rd international Modal Analysis Conference*, volume 1, pages 272–278.
- [24] Smith, J. O. (1992). Physical modeling using digital waveguides. *Computer music journal*, 16(4):74–91.
- [25] Stoica, P. and Moses, R. L. (2005). *Spectral Analysis of Signals*. Pearson/Pren-tice Hall, Upper Saddle River, New Jersey 07458.
- [26] Stokes, G. G. (1845). On the theories of the internal friction of fluids in motion, and of the equilibrium and motion of elastic solids. *Trans. Cambridge Phil. Soc.*, 8:287–319.

A

Wave solution 3D

In this appendix follows the solution of the viscous wave equation in a cylinder. We start by considering the Laplacian in cylindrical coordinates and move on through using the process of separation of variables. After these steps the boundary conditions are analysed until we finally relate the frequency ω of the wave propagation in terms of time with the solutions in the spacial cylindrical coordinates: r , θ and z .

A.1 Cylindrical system

The equation of sound propagation in a viscous fluid is given as [26]

$$\frac{\partial^2 u}{\partial t^2} = c^2 \nabla^2 u + \nu \frac{\partial}{\partial t} \nabla^2 u. \quad (\text{A.1})$$

In order to find a solution to this in a cylindrical system we transform variables to cylindrical coordinates, in which the Laplace operator becomes [22, p. 252]

$$\frac{1}{r} \frac{\partial}{\partial r} \left(r \frac{\partial u}{\partial r} \right) + \frac{1}{r^2} \frac{\partial^2 u}{\partial \theta^2} + \frac{\partial^2 u}{\partial z^2}. \quad (\text{A.2})$$

To solve equation (A.1) we can use the method of separation of variables and we propose a function u on the form

$$u(r, \theta, z, t) = R(r)\Theta(\theta)Z(z)T(t). \quad (\text{A.3})$$

Inserting this ansatz in equation (A.1) in cylindrical coordinates we obtain

$$\frac{T''}{T} = \left(\left(R'' + \frac{1}{r} R' \right) \frac{1}{R} + \frac{1}{r^2} \frac{\Theta''}{\Theta} + \frac{Z''}{Z} \right) \left(c^2 + \nu \frac{T'}{T} \right). \quad (\text{A.4})$$

From here we can collect all terms of T on the left-hand side, in order to get

$$\frac{T''}{c^2T + \nu T'} = \left(\left(R'' + \frac{1}{r}R' \right) \frac{1}{R} + \frac{1}{r^2} \frac{\Theta''}{\Theta} + \frac{Z''}{Z} \right). \quad (\text{A.5})$$

Now, we realise that the right-hand side of this equation is independent of time, t , and we can thus let

$$\frac{T''}{c^2T + \nu T'} = -k^2 \quad (\text{A.6})$$

and solve this sub equation in T . The equation can also be written as

$$T'' + k^2\nu T' + k^2c^2T = 0. \quad (\text{A.7})$$

Assume a solution on the form $T(t) = T_0e^{st}$, where $s \in \mathbb{C}$. Using this ansatz in equation (A.7) yields an equation in s

$$s^2 + sk^2\nu + c^2k^2 = 0, \quad (\text{A.8})$$

with solutions

$$s_{\pm} = \frac{k}{2} \left(k\nu \pm \sqrt{k^2\nu^2 - 4c^2} \right). \quad (\text{A.9})$$

Next we can do the same reasoning on $Z(z)$, where

$$-k^2 - \frac{Z''}{Z} = \left(\left(R'' + \frac{1}{r}R' \right) \frac{1}{R} + \frac{1}{r^2} \frac{\Theta''}{\Theta} \right) = -\kappa^2 \quad (\text{A.10})$$

since the right-hand side is independent of z this time.

The solution to $Z(z)$ is

$$Z(z) = Z_0e^{\pm j\sqrt{k^2 - \kappa^2}z}. \quad (\text{A.11})$$

First multiply both sides of the remaining equation with r^2 in order to free up the Θ -term and let $\frac{\Theta''}{\Theta} = -m^2$ with solution

$$\Theta = \Theta_0e^{\pm jm\theta}, \quad \text{with } m \in \mathbb{N}, \quad (\text{A.12})$$

where we require $m \in \mathbb{N}$ in order to fulfill the 2π -periodicity that we expect from the θ component.

Left is the terms in R and r .

$$r^2R'' + rR' + (r^2\kappa^2 - m^2) = 0 \quad (\text{A.13})$$

can be identified as a Bessel's equation [22, p. 270] with solutions

$$R(r) = J_m(\kappa r) \quad \text{or} \quad R(r) = Y_m(\kappa r), \quad (\text{A.14})$$

where J_m and Y_m are the Bessel functions of the first and second kind respectively. In our case, however, we consider a cylindrical system where we require that the

solution is finite as $r \rightarrow 0$. Thus we can disregard the Y_m :s since these diverge at $r = 0$ zero.

The final variable separated solutions can be summarized as

$$T(t) = T_0 e^{st} \tag{A.15}$$

$$Z(z) = Z_0 e^{\pm j\sqrt{k^2 - \kappa^2}z} \tag{A.16}$$

$$\Theta(\theta) = \Theta_0 e^{jm\theta} \tag{A.17}$$

$$R(r) = R_0 J_m(\kappa r). \tag{A.18}$$

A.1.1 Boundary conditions

In order to relate the solutions to the system at hand we need to consider the boundary conditions.

For the sake of argument, let the cylinder be closed in both ends and have a length of L and a radius a . Variations of these boundary conditions can be treated analogously.

We start by looking at this boundary condition in terms of the radial function. This needs to be zero at $r = a$, which implies that $J_m(\kappa a) = 0$. However $J_m(x)$ oscillate around zero and there are thus several solutions to this equation, so let us number the roots as n . Then the solutions are given as $\kappa_{m,n}$, which can be solved numerically for every m and n .

With $\kappa_{m,n}$ set we can move on to consider the boundary in z -direction. This becomes $Z(z = 0) = Z(z = L) = 0$ and we can select the sine term of the complex exponential in order to achieve this. However, that also requires that $\sqrt{k^2 - \kappa^2}L = l\pi$, where $l \in \mathbb{N}$. Thus

$$k_{m,n,l} = \pm \sqrt{\kappa_{m,n}^2 + \left(\frac{l\pi}{L}\right)^2}. \tag{A.19}$$

A.1.2 Attenuation and resonance

Further we can decompose the complex number $s = \sigma \pm j\omega$ in order to find the fundamental frequencies, $\omega_{m,n,l}$, of the system. If we require a travelling wave solution we get the condition that $4c^2 > k^2\nu^2$ and the term under the square root in the solution to s becomes negative and we can then identify

$$\sigma = -\frac{k^2\nu}{2} \quad \text{and} \quad \omega = \frac{k}{2}\sqrt{4c^2 - k^2\nu^2}. \tag{A.20}$$

B

System identification

THE following appendix provides a detailed description of a method for solving the linear optimisation problem defined in equation (2.34). The main idea is to pose the optimisation problem as a least squares estimation (LSE) problem, which can then be solved using conventional LSE methods [1].

B.1 Linear optimisation

The aim is to find a parameter vector, $\hat{\theta}^*$, fulfilling the inclusion

$$\hat{\theta}^* \in \operatorname{argmin}_{\theta} \sum_{k=1}^N |A(j\omega_k, \theta)\check{H}(\omega_k) - B(j\omega_k, \theta)|^2 \frac{|W(\omega_k)|^2}{|A^*(j\omega_k)|^2}. \quad (\text{B.1})$$

First we can use the fact that A and B are polynomials in $j\omega$ with the coefficients contained in the parameter vector θ . Let us make the assumption that

$$A(j\omega_k, \theta) = 1 + \sum_{l=1}^{N_a} a_l (j\omega_k)^l \quad \text{and} \quad B(j\omega_k, \theta) = b_0 + \sum_{l=1}^{N_b} b_l (j\omega_k)^l, \quad (\text{B.2})$$

where N_a and N_b is the degree of each polynomial, respectively. we define the parameter vector, $\theta \in \mathbb{C}^{N_a+N_b+1}$, as

$$\theta = \begin{bmatrix} a_1 \\ \vdots \\ a_{N_a} \\ b_0 \\ \vdots \\ b_{N_b} \end{bmatrix}. \quad (\text{B.3})$$

Further to reduce the equation to matrix form we define

$$\Omega^{(k)} = \begin{bmatrix} -(j\omega)\check{H}(\omega_k) \\ \vdots \\ -(j\omega)^{N_a}\check{H}(\omega_k) \\ 1 \\ (j\omega) \\ \vdots \\ (j\omega)^{N_b} \end{bmatrix}, \quad k = 1, \dots, N, \quad (\text{B.4})$$

which means that the inner expression in (B.1) can be rewritten as

$$|A(j\omega_k, \theta)\check{H}(\omega_k) - B(j\omega_k, \theta)| = |\check{H}(\omega_k) - (\Omega^{(k)})^T \theta|. \quad (\text{B.5})$$

Next we can reformulate the sum over the frequencies in terms of a vector multiplication. First let

$$\Omega_N = \begin{bmatrix} (\Omega^{(1)})^T \frac{|W(\omega_1)|}{|A^*(j\omega_1)|} \\ \vdots \\ (\Omega^{(N)})^T \frac{|W(\omega_N)|}{|A^*(j\omega_N)|} \end{bmatrix}. \quad (\text{B.6})$$

The objective function, which should be minimised, can now be rewritten as

$$V_N(\theta) = \sum_{k=1}^N |\check{H}(\omega_k) \frac{|W(\omega_k)|}{|A^*(j\omega_k)|} - (\Omega^{(k)})^T \theta|^2. \quad (\text{B.7})$$

In order to find the parameter vector, $\hat{\theta}^*$, which minimises the function, $V_N(\theta)$, we consider the gradient with respect to the parameters and setting that to zero, i.e.,

$$\nabla V_N(\theta) = \sum_{k=1}^N 2(\Omega^{(k)}) \check{H}(\omega_k) \frac{|W(\omega_k)|}{|A^*(j\omega_k)|} - (\Omega^{(k)})^T \theta = 0. \quad (\text{B.8})$$

To fulfill equation (B.8), it must hold that

$$\sum_{k=1}^N (\Omega^{(k)}) \check{H}(\omega_k) \frac{|W(\omega_k)|}{|A^*(j\omega_k)|} = \sum_{k=1}^N (\Omega^{(k)}) (\Omega^{(k)})^T \theta. \quad (\text{B.9})$$

If we now let $Y^{(k)} = \check{H}(\omega_k) \frac{|W(\omega_k)|}{|A^*(j\omega_k)|}$ and

$$Y_N = \begin{bmatrix} Y^{(1)} \\ \vdots \\ Y^{(N)} \end{bmatrix}, \quad (\text{B.10})$$

equation (B.9) can be rewritten on matrix form according to

$$\Omega_N^T Y_N = \Omega_N^T \Omega_N \theta \quad (\text{B.11})$$

The parameter vector, $\hat{\theta}^*$, fulfilling equation (B.11) can now be computed by

$$\hat{\theta}^* = (\Omega_N^T \Omega_N)^{-1} \Omega_N^T Y_N = \Omega_N^\dagger Y_N, \quad (\text{B.12})$$

where Ω_N^\dagger is the pseudo inverse of Ω_N .